Cancer Cell

Article

Intratumoral CD8+ T cells with a tissue-resident memory phenotype mediate local immunity and immune checkpoint responses in breast cancer

Graphical abstract

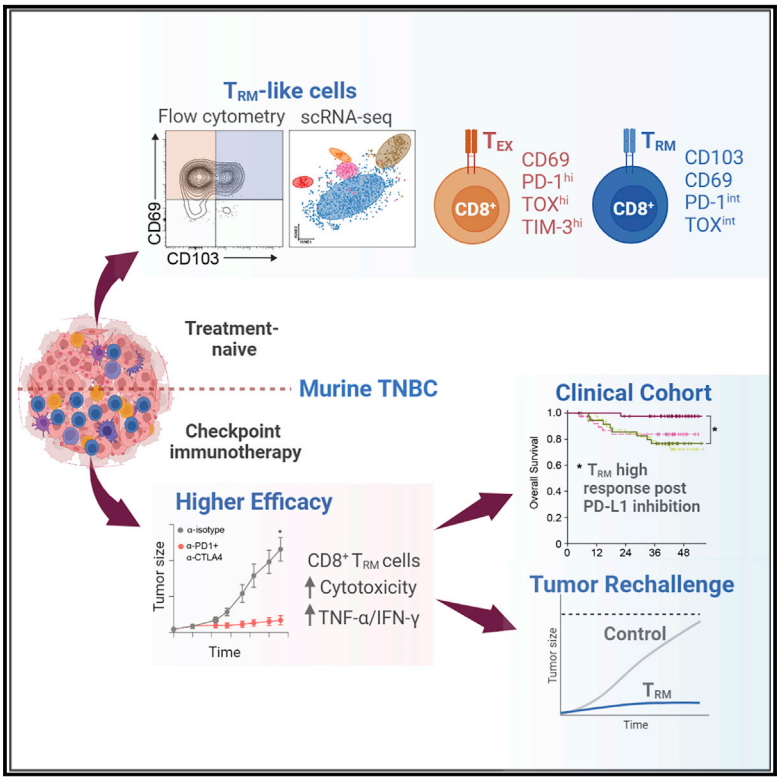

Highlights

- Intratumoral CD8+ T cells in murine TNBC consist of both T_{EX}-like and T_{RM}-like cells
- Dual-ICB therapy augments and enhances the killing capacity of T_{RM}-like cells
- CD8+ T_{RM}-like cells provide local tissue protection from TNBC tumor rechallenge
- CD8+ T_{RM} signature is associated with better treatment outcomes in TNBC patients

Authors

Balaji Virassamy, Franco Caramia, Peter Savas, ..., Paul J. Neeson, Laura K. Mackay, Sherene Loi

Correspondence

phil.darcy@petermac.org (P.K.D.), paul.neeson@petermac.org (P.J.N.), lkmackay@unimelb.edu.au (L.K.M.), sherene.loi@petermac.org (S.L.)

In brief

Virassamy et al. characterize the qualitative features of intratumoral CD8+ T cells and the critical role of T cells displaying residency properties (T_{RM}) in mouse models of triple-negative breast cancer (TNBC). T_{RM} cells expand in response to anti-PD-1 and anti-CTLA-4 immune checkpoint inhibition and confer ongoing tissue protective immunity against TNBC.

Virassamy et al., 2023, Cancer Cell *41*, 585–601
March 13, 2023
https://doi.org/10.1016/j.ccell.2023.01.004

CellPress

Cancer Cell

CellPress

Article

Intratumoral CD8+ T cells with a tissue-resident memory phenotype mediate local immunity and immune checkpoint responses in breast cancer

Balaji Virassamy,[1] Franco Caramia,[1] Peter Savas,[1,2] Sneha Sant,[1,2] Jianan Wang,[3,4] Susan N. Christo,[4,5] Ann Byrne,[1] Kylie Clarke,[1] Emmaline Brown,[1] Zhi Ling Teo,[1,2] Bianca von Scheidt,[1] David Freestone,[5] Luke C. Gandolfo,[3,5] Karsten Weber,[6] Julia Teply-Szymanski,[6,7] Ran Li,[1] Stephen J. Luen,[1,2] Carsten Denkert,[6,7] Sibylle Loibl,[6] Olivia Lucas,[8,9,10] Charles Swanton,[8,9] Terence P. Speed,[3,11] Phillip K. Darcy,[1,2,12,*] Paul J. Neeson,[1,2,12,*] Laura K. Mackay,[4,5,12,*] and Sherene Loi[1,2,12,13,*]

[1]Division of Cancer Research, Peter MacCallum Cancer Centre, Melbourne, VIC, Australia
[2]The Sir Peter MacCallum Department of Medical Oncology, University of Melbourne, Melbourne, VIC, Australia
[3]Bioinformatics Division, Walter and Eliza Hall Institute of Medical Research, Melbourne, VIC, Australia
[4]Department of Medical Biology, The University of Melbourne, Melbourne, VIC, Australia
[5]Department of Microbiology and Immunology, The University of Melbourne at the Peter Doherty Institute for Infection and Immunity, Melbourne, VIC, Australia
[6]German Breast Cancer Group, GBG-Forschungs GmbH, Neu-Isenburg, Germany
[7]Department of Pathology, University Marburg-Giessen, Campus Marburg, Germany
[8]Cancer Evolution and Genome Instability Laboratory, The Francis Crick Institute, London, UK
[9]Cancer Research UK Lung Cancer Centre of Excellence, University College London Cancer Institute, London, UK
[10]Computational Cancer Genomics Research Group, University College London Cancer Institute, London, UK
[11]School of Mathematics and Statistics, University of Melbourne, Melbourne, VIC, Australia
[12]Senior authors
[13]Lead contact
*Correspondence: phil.darcy@petermac.org (P.K.D.), paul.neeson@petermac.org (P.J.N.), lkmackay@unimelb.edu.au (L.K.M.), sherene.loi@petermac.org (S.L.)
https://doi.org/10.1016/j.ccell.2023.01.004

SUMMARY

CD8+ tumor-infiltrating lymphocytes with a tissue-resident memory T (T_{RM}) cell phenotype are associated with favorable prognosis in patients with triple-negative breast cancer (TNBC). However, the relative contribution of CD8+ T_{RM} cells to anti-tumor immunity and immune checkpoint blockade efficacy in breast cancer remains unknown. Here, we show that intratumoral CD8+ T cells in murine mammary tumors transcriptionally resemble those from TNBC patients. Phenotypic and transcriptional studies established two intratumoral sub-populations: one more enriched in markers of terminal exhaustion (T_{EX}-like) and the other with a bona fide resident phenotype (T_{RM}-like). Treatment with anti-PD-1 and anti-CTLA-4 therapy resulted in expansion of these intratumoral populations, with the T_{RM}-like subset displaying significantly enhanced cytotoxic capacity. T_{RM}-like CD8+ T cells could also provide local immune protection against tumor rechallenge and a T_{RM} gene signature extracted from tumor-free tissue was significantly associated with improved clinical outcomes in TNBC patients treated with checkpoint inhibitors.

INTRODUCTION

Tissue-resident memory T (T_{RM}) cells reside in healthy peripheral tissues where they form the first line of defense against invading pathogens.[1–4] T_{RM} cells were originally described in peripheral tissues following murine viral infection[5,6] and have subsequently been described within most organs in humans and mice.[7,8] Unlike central memory T (T_{CM}) cells and effector memory T (T_{EM}) cells that continuously circulate between peripheral tissues and lymph nodes, T_{RM} cells persist in localized tissues where they play a critical role in local immunosurveillance.[1,5,9,10] While CD8+ T_{RM} cells exhibit heterogeneity between organs, they share a common transcriptional signature that differentiates them from T cells in the circulation, and they are typically characterized by surface expression of CD69 and CD103 in tissues and tumors.[11–17] In addition, the presence of CD103+CD8+ T_{RM} cells in tumors has been strongly correlated with favorable outcomes in several human solid cancers.[14,16–21] Furthermore, CD103+CD8+ T_{RM} cells have been shown to accumulate in the tumor microenvironment following anti-PD-1 therapy, which improved melanoma patient survival,[18] promoted anti-tumor immune responses[22] and immunosurveillance in preclinical melanoma models.[23,24] However,

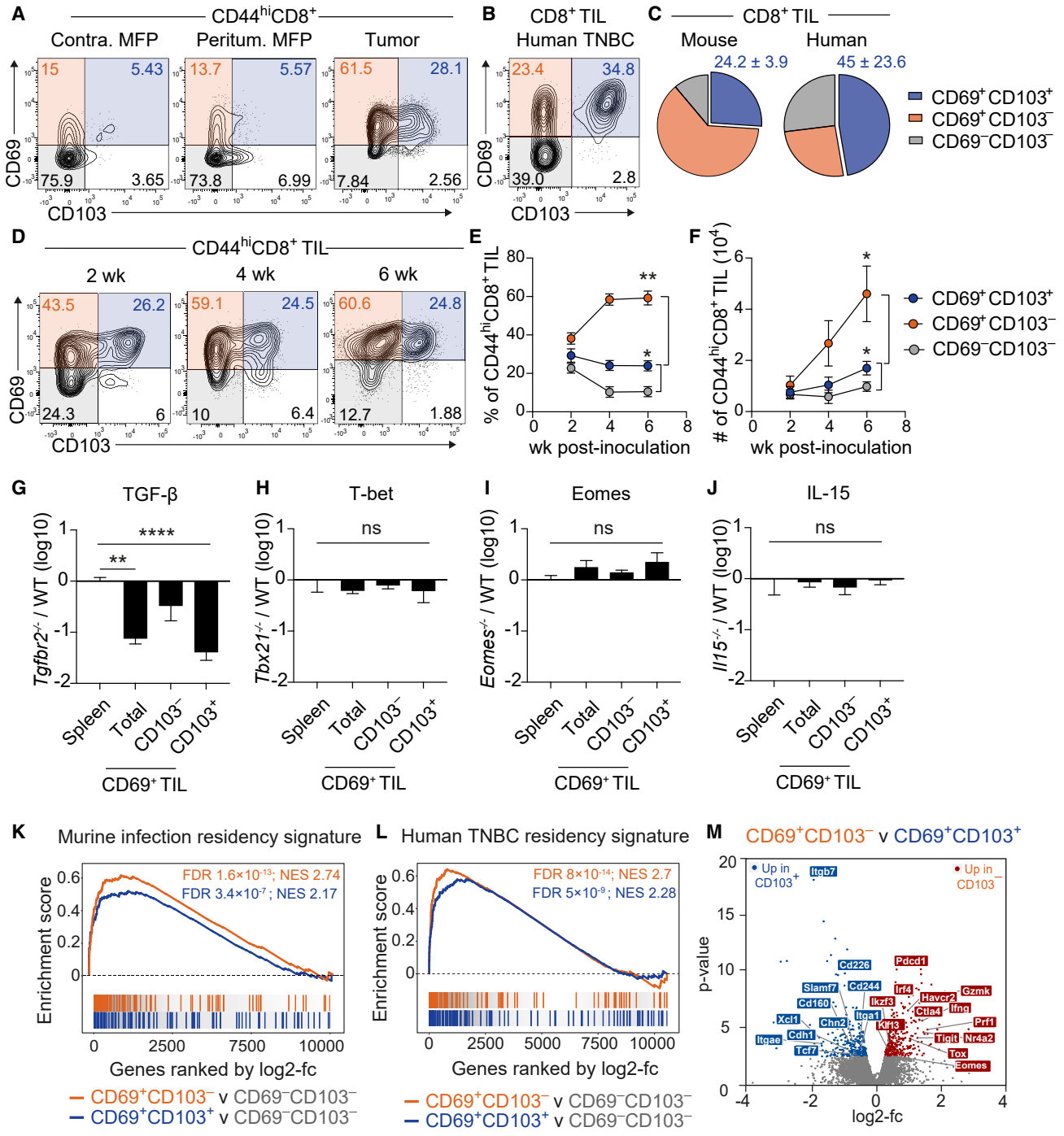

Figure 1. CD8⁺ T_{RM}-like cells in murine TNBC transcriptionally resemble T_{RM} cells across murine tissues and human TNBC

(A) Representative CD69 and CD103 expression on T_{RM}-like CD44^{hi}CD8^{+} T cells in contralateral, peritumoral and tumor tissues at 4 weeks post AT3-OVA inoculation.

(B) Representative CD69 and CD103 expression on CD45RA^{-}CCR7^{-} CD8^{+} T cells in primary human TNBC tumors.

(C) Percentage of T cells with CD69^{+}CD103^{+} T_{RM}-like phenotype in mouse (n = 8) and human CD8^{+} TILs (n = 10). Data indicate mean ± SD.

(D) Representative CD69 and CD103 expression on T_{RM}-like CD44^{hi}CD8^{+} T cells infiltrating tumors at 2, 4, and 6 weeks post AT3-OVA inoculation.

(E and F) Percentage and number of CD69^{+}CD103^{+} (blue), CD69^{+}CD103^{-} (orange), and CD69^{-}CD103^{-} (gray) CD8^{+} TILs at 2, 4, and 6 weeks post AT3-OVA inoculation. (n = 6–8) Mean ± SEM. Unpaired two-tailed Student's t test.

(G–J) OT-I TILs were analyzed on day 30 following equal number of naive OT-I.CD45.1.2. wild-type (WT) and OT-I.CD45.1.TGF-β receptor(R) II$^{-/-}$(*Tgfbr2*$^{-/-}$) or OT-I.CD45.1.*Tbx21*$^{-/-}$(*Tbx21*$^{-/-}$) or OT-I.CD45.1.*Eomes*$^{-/-}$(*Eomes*$^{-/-}$) T cells or effector CD45.2.*Il15*$^{-/-}$(*Il15*$^{-/-}$) were transferred to CD45.2 recipient mice prior

(legend continued on next page)

the role for T_{RM} cells and the markers to identify these cells in this context for breast cancer, a tumor type generally considered to have a "colder" tumor microenvironment, remains poorly understood.

Triple-negative breast cancer (TNBC) is an aggressive cancer subtype that accounts for approximately 15%–20% of all breast cancers and is associated with poor survival outcomes.[25,26] Despite not being traditionally thought of as an immunogenic type of cancer with relatively low tumor mutational burden, the presence of a high number of tumor-infiltrating lymphocytes (TILs) in TNBC is associated with significantly better outcomes with and without PD-1 targeting immunotherapy.[27,28] While breast cancer TIL predominantly contains $CD3^+$ T cells,[29,30] we recently reported the presence of a sub-population of $CD8^+$ T cells with a T_{RM}-like phenotype using single-cell RNA sequencing (scRNA-seq) of $CD3^+$ T cells isolated from human primary TNBCs.[13] $CD8^+$ T_{RM}-like cells expressed high levels of immune checkpoint molecules, such as *PDCD1* (PD-1), *CTLA4*, *HAVCR2* (TIM-3), and *LAG3,* and the transcriptional signature derived from these cells was associated with a better prognosis independent of the quantity of total $CD8^+$ T cells present and treatment given.[13,31]

Immune checkpoint therapy has been revolutionary for multiple cancer types, particularly the more immunogenic solid cancers such as melanoma and non-small cell lung cancer.[32] Immune checkpoint inhibitors such as anti-PD-1 and anti-CTLA-4 block suppressive signals for T cell function leading to an effective anti-tumor response partly mediated by $CD8^+$ T cells.[33,34] It is well recognized that the clinical efficacy of checkpoint inhibitors is associated with the quantity of pre-existing $CD8^+$ TILs.[35] Studies in human melanoma and non-small cell lung cancer samples have shown a positive correlation of $CD8^+$ T_{RM} cells with favorable outcomes following anti-PD-1 therapy.[36–38] However, the role of $CD8^+$ T_{RM} cells in this context, and the heterogeneity among tumor-resident $CD8^+$ T cell sub-populations in breast cancer remains unclear.

Recently, atezolizumab (anti-PD-L1) and pembrolizumab (anti-PD-1) have been approved in the treatment of early- and late-stage TNBC, with PD-L1 protein expression as the approved companion biomarker.[27,39–42] Given the high expression of immune checkpoint molecules on $CD8^+$ T_{RM} cells in human TNBCs, we hypothesized that these cells may be a critical target for therapeutic modulation within the tumor microenvironment. Supporting this, we have recently reported that the gene signature derived from $CD8^+$ T_{RM} cells derived from human TNBC was significantly associated with response to pembrolizumab in patients.[43] In this current study, we sought to understand the role of $CD8^+$ T_{RM} cells in breast cancer, particularly in the context of immune checkpoint blockade and immunosurveillance. To this end, we used a murine model of syngeneic TNBC tumors that develop in the mammary fat pad and describe the development of intratumoral $CD8^+$ T cells that arise during mammary tumor formation. We describe the critical role of a subset with tissue-resident properties in breast cancer in the setting of immune checkpoint blockade, as well as their role in ongoing breast cancer immune surveillance after tumor rechallenge.

RESULTS

Intratumoral $CD8^+$ T cells in murine mammary cancers transcriptionally resemble T_{RM} cells from healthy tissues and from human TNBC

We have previously shown the prevalence of $CD103^+CD8^+$ T_{RM} cells in early-stage human TNBCs and their strong association with improved patient prognosis.[13] To characterize $CD8^+$ T_{RM} cell development in breast cancer, we used a murine model of TNBC, where syngeneic transplantable AT3-OVA tumor cells were orthotopically injected in the fourth mammary fat pad (MFP) of C57BL/6J mice. Four weeks after AT3-OVA tumor inoculation, TILs were isolated from established mammary tumors and assessed for $CD44^{hi}CD8^+$ T cell sub-populations expressing the canonical markers of tissue-residency CD69 and CD103. The $CD69^+CD103^+CD8^+$ T cells were predominantly present in tumor tissue compared with peritumoral or naive contralateral MFP (Figure 1A). Furthermore, based on CD69 and CD103 expression, these T cell subsets could be detected in $CD8^+$ TILs in both the AT3-OVA model and human TNBCs (Figures 1B and 1C). We next tracked the temporal development of these T cell populations following AT3-OVA tumor inoculation (Figure 1D). We observed that $CD44^{hi}CD8^+$ T cells that expressed CD69 alone or co-expressed CD69 and CD103 were significantly higher in proportion and quantity relative to $CD69^-CD103^-$ T cells over the 6-week period (Figures 1E and 1F). This corresponded with a concomitant decline in the proportion of $CD69^-CD103^-$ T cells indicating a loss of these cells or conversion to the $CD69^+$ phenotype over time (Figure 1F). Further assessment of OVA antigen-specific $CD8^+$ TIL revealed a substantial proportion of H-$2K^b$ $OVA_{(257-264)}$ $tetramer^+$ staining present in all three T cell populations, with a significantly higher proportion of $tetramer^+$ cells observed in the $CD69^+CD103^-$ compared with $CD69^+CD103^+$ and $CD69^-CD103^-$ populations (Figures S1A and S1B).

to AT3-OVA inoculation. The total ratio of $CD69^+$ TIL, $CD69^+CD103^-$, and $CD69^+CD103^+$ TIL phenotypes by (G) *Tgfbr2*$^{-/-}$, (H) *Tbx21*$^{-/-}$, (I) *Eomes*$^{-/-}$ and (J) *Il15*$^{-/-}$ (n = 9–10). Two-tailed Mann-Whitney test.

(K–M) Intratumoral $CD69^-CD103^-$, $CD69^+CD103^-$, and $CD69^+CD103^+$ $CD8^+$ T cell sub-populations were FACS sorted at 6 weeks post BC inoculation and analyzed by RNA-seq. GSEA of DEGs between $CD69^+CD103^-$ vs. $CD69^-CD103^-$ and $CD69^+CD103^+$ vs. $CD69^-CD103^-$ sub-populations are shown.

(K) $CD69^+CD103^-$ (orange) and $CD69^+CD103^+$ (blue) T cell populations with enrichment of 85 $CD8^+$ T_{RM} associated genes that were upregulated in "murine infection residency signature" derived from Mackay et al.[44] False discovery rate (FDR) by gene set test.

(L) $CD69^+CD103^-$ (orange) and $CD69^+CD103^+$ (blue) T cell phenotypes with enrichment of 141 $CD8^+$ T_{RM} upregulated genes that were filtered based on FDR <0.01 and log fold change >1 "Human TNBC T_{RM} signature" from Savas et al.[13] Data presented as log2-fold change (fc) from n = 3 biologically independent experiments.

(M) Volcano plot of DEGs between $CD69^+CD103^-$ and $CD69^+CD103^+$ TIL phenotypes with significantly upregulated genes in $CD69^+CD103^-$ T cells (red) and significantly upregulated genes in $CD69^+CD103^+$ T cells (blue) with FDR <0.05 are shown from n = 3 independent experiments. *p < 0.05; **p < 0.01; ****p < 0.0001, ns, not significant.

See also Figures S1 and S2, and Table S1.

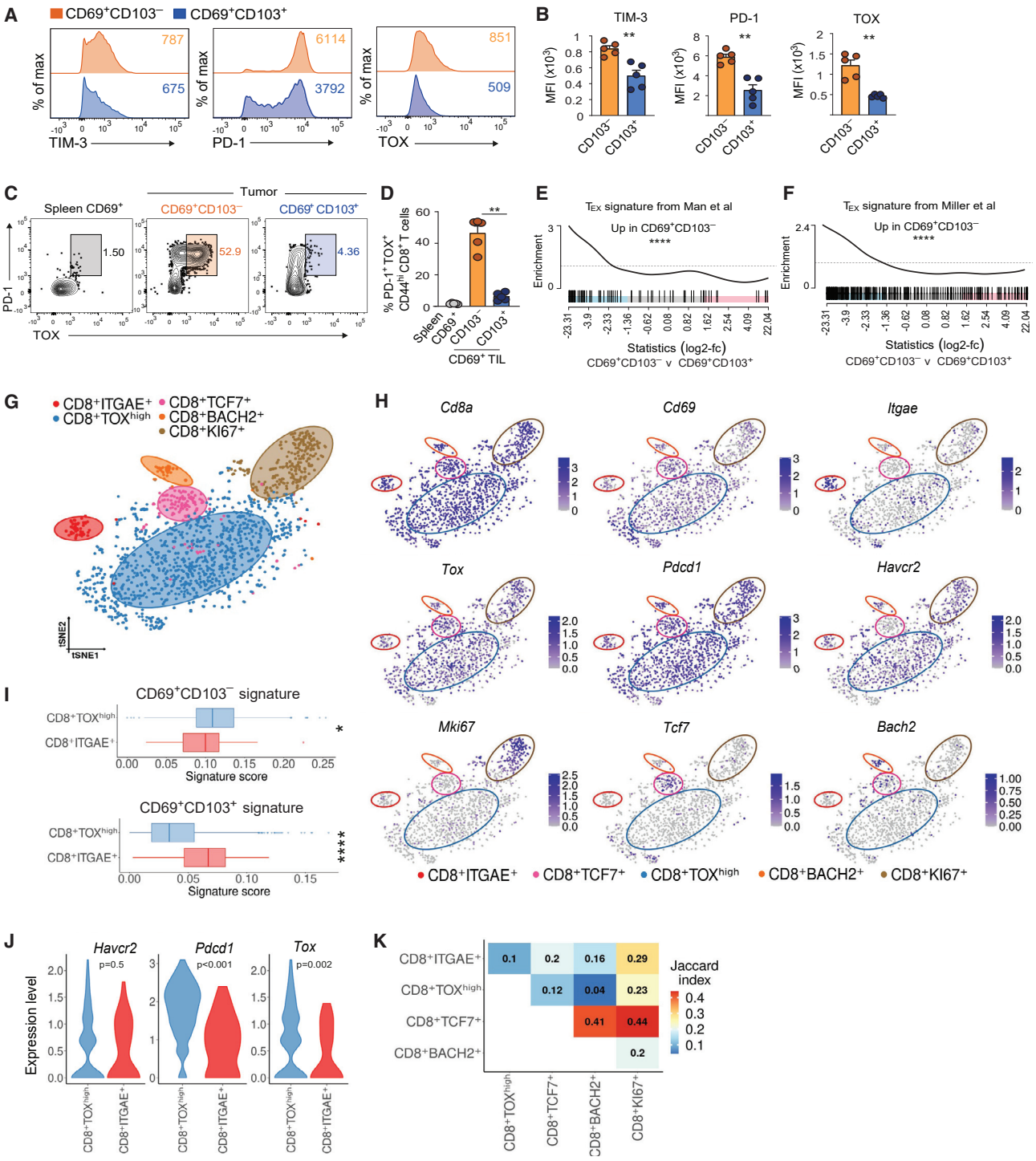

Figure 2. TNBC tumors contain phenotypically and transcriptionally distinct CD8⁺ T cell sub-populations

(A) Representative histograms of TIM-3, PD-1, and TOX between CD69⁺CD103⁻ (orange) and CD69⁺CD103⁺ (blue) CD44^{hi}CD8⁺ TILs isolated from week 4 AT3-OVA tumors.

(B) Mean fluorescence intensity (MFI) expression of TIM-3, PD-1, and TOX among CD69⁺CD103⁻ and CD69⁺CD103⁺ CD8⁺ TIL sub-populations, (n = 5) mean ± SEM. Two-tailed Mann-Whitney test.

(C) PD-1 and TOX expression among spleen CD69⁺CD44^{hi}CD8⁺ T cells and intratumoral CD69⁺CD103⁻ and CD69⁺CD103⁺ CD44^{hi}CD8⁺ T cell sub-populations.

(D) Percentage of PD-1 and TOX co-expression among spleen CD69⁺CD44^{hi}CD8⁺ T cells and intratumoral CD69⁺CD103⁻ and CD69⁺CD103⁺ CD44^{hi}CD8⁺ T cell sub-populations. Data indicate mean ± SEM, shown from one of two experiments, n = 5 mice. Two-tailed Mann-Whitney test.

(legend continued on next page)

$CD8^+$ T_{RM} cell differentiation is dependent on molecular cues that are distinct from those that drive circulating $CD8^+$ T cell populations and the signaling requirements vary in different tissues.[4,45,46] The molecular signals that govern the differentiation of T_{RM} cells in breast cancer are currently unknown. Transforming growth factor (TGF)-β is required for T_{RM} cell development in several tissues,[3,47–49] as well as for driving CD103 expression.[50,51] In adoptive transfer experiments using OT-I T cells that lacked expression of the TGF-β receptor(R)II (OT-I.*Tgfbr2*$^{-/-}$), we found that $CD69^+$ TGF-βRII-deficient OT-I T cells were significantly reduced in mammary tumors compared with wild-type controls, demonstrating the requirement of TGF-β for the development of TNBC $CD8^+$ T_{RM} cell populations (Figure 1G). The T-box transcription factor T-bet is essential for T_{RM} cell survival in tissues including the skin and lung.[46,52] To determine the dependence of TNBC T_{RM} cells on T-box transcription factors, we co-transferred wild-type OT-I T cells (OT-I.WT) and T-bet or Eomes deficient OT-I T cells (OT-I.*Tbx21*$^{-/-}$or OT-I.*Eomes*$^{-/-}$, respectively) into mice prior to challenge with AT3-OVA tumor cells. We found that $CD8^+CD69^+$ TIL cells were not numerically altered in the absence of T-bet and Eomes (Figures 1H and 1I). T-box transcription factors act in part via the control of interleukin (IL)-15 responsiveness,[46,53] and consistent with this, we found that mammary tumor T_{RM} were also not reliant on this cytokine (Figure 1J) compared with T_{RM} cells in other tissue sites.[46,54–56]

To assess the changes in the transcriptional profile of $CD69^+CD103^-$ and $CD69^+CD103^+$ $CD8^+$ T cells, we tracked the development of these $CD8^+$ T cell sub-populations from developing tumors at 2, 4, and 6 weeks and analyzed these cells by bulk RNA-seq. Two weeks after tumor inoculation, we found that genes that have been previously associated with T_{RM} cells across normal tissues[3] were expressed by both $CD69^+CD103^-$ and $CD69^+CD103^+$ populations, for example, the upregulation of *Itgae, Itga1, Cd244a, Cdh1, Chn2, Qpct, Rgs2,* and *Nr4a2* and downregulation of *S1pr1*, *S1pr5,* and *Eomes*, as compared with the $CD69^-CD103^-$ population (Figures S1C and S1D). Furthermore, we found that the transcriptomes of $CD69^+CD103^-$ and $CD69^+CD103^+$ T cells were significantly enriched for a transcriptional signature derived from $CD8^+$ T_{RM} cells from the skin, gut, and liver of mice following resolution of viral infection[44] (Figure 1K), and also a $CD8^+$ T_{RM} cell gene signature extracted from early-stage human TNBC tumors[13] (Figure 1L). Collectively, our data suggest that qualitatively distinct intratumoral $CD8^+$ T cell phenotypes develop in the AT3-OVA murine mammary model and that the transcriptional profile of $CD69^+CD103^-$ and $CD69^+CD103^+$ $CD8^+$ T cells resemble $CD8^+$ T_{RM} cells following resolution of acute infection from healthy murine tissues, as well as those extracted from human primary TNBCs. In addition, we examined other murine BC models for the presence of CD69 and CD103 residency markers on $CD44^+CD8^+$ T cells. We found that these cell populations exist at a lower level in the 4T1 model (13%) and are negligible in the E0771-OVA (5%) nor in EO771 (4%) parental tumors (Figures S2A and S2B). The 4T1 model is known to be myeloid dominant, highly metastatic, and does not respond to anti-PD-1 therapy,[57,58] while the E0771 model is thought to be more representative of luminal rather than basal-like breast cancers.[59] The intratumoral $CD8^+$ T cell sub-populations in both 4T1 and AT3 parental tumors co-expressed the immune checkpoint receptor PD-1 (Figure S2C).

Although both $CD69^+CD103^-$ and $CD69^+CD103^+$ cells bore transcriptional similarities to T_{RM} cells, we observed a significant difference in gene expression profiles between these two populations. We found 304 significantly upregulated genes in $CD69^+CD103^-$ and 297 significantly upregulated in $CD69^+CD103^+$ cells (Figure 1M, Table S1). Specifically, we observed that genes associated with T cell exhaustion, such as *Tox, Eomes, Havcr2* (TIM-3), *Pdcd1* (PD-1), and *Ctla4* were significantly upregulated in the $CD69^+CD103^-$ sub-population, whereas genes associated with tissue residency, such as *Cdh11, Chn2, Cd244, Xcl1,* and *Itga1* were significantly upregulated in the $CD69^+CD103^+$ population.

Intratumoral $CD69^+CD8^+$ T cells in murine mammary cancers contain both exhausted (T_{EX}) and resident (T_{RM}) memory-like phenotypes

$CD8^+$ T_{RM} cells have been shown to play a critical role in anti-tumor immunity and cancer immune surveillance in other cancer types.[24,60] In our murine model, the $CD44^{hi}CD8^+$ T cells from AT3-OVA mammary tumors comprised two distinct subgroups: $CD69^+CD103^-$ cells that expressed genes more associated with exhaustion, and $CD69^+CD103^+$ cells, which exhibited a gene signature more suggestive of bona fide tissue residency. In line with the differential gene expression analyses, surface protein evaluation confirmed elevated expression of TOX, TIM-3, and PD-1 by $CD69^+CD103^-$ cells compared with $CD69^+CD103^+$ cells (Figures 2A and 2B), as well as a greater proportion of $CD69^+CD103^-$ cells co-expressing PD-1 and TOX (Figures 2C and 2D). Corroborating the notion that the $CD69^+CD103^-$ population exhibited features characteristic of terminal exhaustion, we found that the transcriptome of these cells was significantly enriched with two independent gene signatures derived from T_{EX} cells[61,62] (Figures 2E and 2F). Together,

(E) GSEA indicating $CD69^+CD103^-$ compared with $CD69^+CD103^+$ $CD44^{hi}CD8^+$ TIL phenotype with significant enrichment of genes associated with "Core $CD8^+$ T cell exhaustion signature" derived from chronic LCMV infection, Man et al[61] n = 3. FDR by gene set test.
(F) GSEA indicating $CD69^+CD103^-$ compared with $CD69^+CD103^+$ $CD44^{hi}CD8^+$ TIL phenotype with significant enrichment of genes associated with "Terminally exhausted $CD8^+$ T cells" derived from chronic LCMV infection,[62] n = 3, FDR by gene set test.
(G–K) Single-cell RNA-seq of $CD8^+$ TILs (n = 1,548) isolated from mammary tumors at 2 weeks post AT3-OVA inoculation.
(G) t-SNE plot demonstrating five distinct $CD8^+$ T cell clusters indicated by colored ellipses.
(H) Feature plots with key genes among $CD8^+$ T cell clusters.
(I) Significant enrichment of week 6 AT3-OVA derived $CD69^+CD103^-$ $CD8^+$ T_{EX} signature and $CD69^+CD103^+$ $CD8^+$ T_{RM} signature in the $CD8^+ITGAE^+$ cluster and $CD8^+TOX^+$ clusters. FDR by gene set test.
(J) Expression of *Havcr2* (TIM-3), *Pdcd1* (PD-1), and *Tox* gene transcripts in $CD8^+TOX^{high}$ and $CD8^+ITGAE^+$ clusters. Wilcoxon rank-sum test.
(K) Jaccard indices showing the relatedness of TCR repertoires among $CD8^+$ T cell clusters. Jaccard coefficient with 0 indicating no overlap and 1 complete overlap of TCR sequences among pairs of clusters from n = 3 murine tumors. $^{**}p < 0.01$; $^{****}p < 0.0001$ and each symbol represents an individual mouse.
See also Tables S2 and S3.

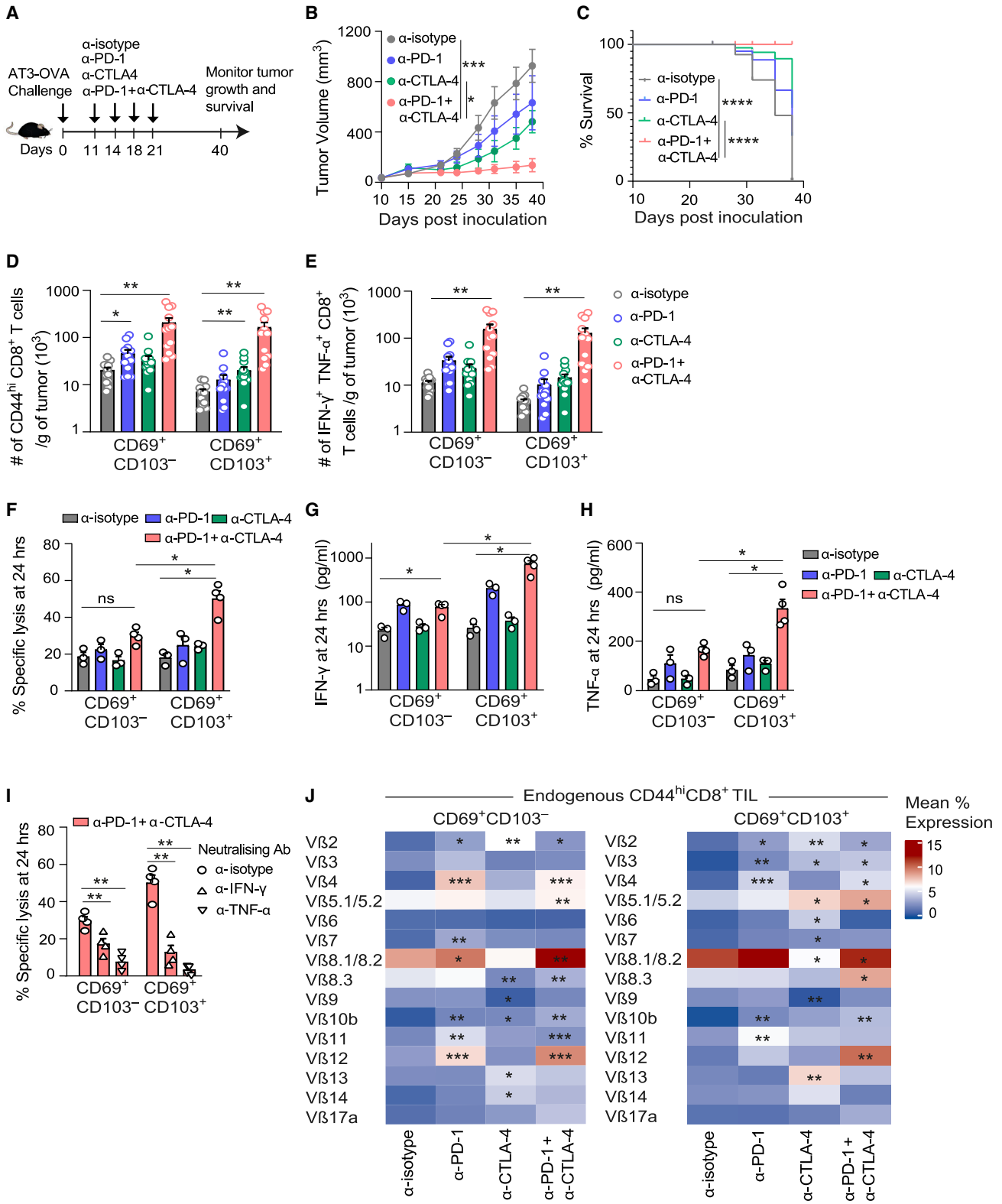

Figure 3. Dual-ICB therapy induces qualitative and quantitative changes in CD69$^+$CD103$^+$ CD8$^+$ T_{RM}-like cells, which associates with BC tumor control

(A) Schematic diagram with treatment schedule.

(B) AT3-OVA BC tumor growth curve following indicated ICB treatments, n = 10 mice shown from two independent experiments, mean ± SEM and statistics determined on day 38. Two-way ANOVA with Turkey's multiple comparisons test.

(legend continued on next page)

these data reveal the phenotypic differences between $CD69^+CD103^-$ and $CD69^+CD103^+$ T cell populations, with the latter likely being more resident-like and the former displaying markers of exhausted (T_{EX}) T cells.

To examine these intratumoral T cell sub-populations in an unbiased manner, we generated scRNA-seq data from 1,548 single $CD8^+$ T cells extracted from established mammary tumors 2 weeks post AT3-OVA inoculation. T cell clusters were visualized using t-distributed stochastic neighbor embedding (t-SNE) plots (Figure 2G). We observed five distinct clusters, including a cluster that could be characterized by elevated *Itgae* (encodes for CD103) expression (red) as well as one that had high expression of *Tox* (blue) (Figures 2G and 2H). Clusters *Itgae* vs. *Tox* were significantly enriched with the genes differentially expressed between $CD69^+CD103^+$ compared with $CD69^+CD103^-$ cells, respectively (Figure 2I, Table S2), with lower expression of *Havcr2 (TIM-3)* and *Pdcd1* in the *Itgae* vs. *Tox* clusters, respectively (Figure 2J). Interestingly we also noticed a *Tcf7*$^+$ cluster that was molecularly distinct from the *Itgae* vs. *Tox* clusters (Table S3). In addition, we examined for overlap in T cell receptor (TCR) clones between clusters high in *Itgae* and *Tox* respectively. Consistent with our hypothesis, we found little TCR clonal overlap between these two clusters (Figure 2K), suggesting differing antigen specificity. These unbiased single-cell analyses are consistent with and validate our data above: that these intratumoral sub-populations defined by CD103 and CD69 are distinct.

Anti-tumor responses induced by ICB are associated with increased function, quantity, and quality of $CD8^+$ T_{RM}-like cells

We have previously shown that $CD8^+$ T_{RM} cells in human TNBC expressed high levels of immune checkpoint molecules such as PD-1 and CTLA-4.[13] Given the expression of checkpoint molecules on this tumor-resident population, T_{RM} cells are a potential cellular target mediating the therapeutic effects of checkpoint inhibitors.[63] To investigate the therapeutic effect of PD-1 and CTLA-4 blockade, we injected AT3-OVA cells in the MFP of mice and treated them with isotype control antibody, anti-PD-1, anti-CTLA-4, or dual anti-PD-1 and anti-CTLA-4 combination therapy (Figure 3A). Compared with single-agent blockade, dual-ICB therapy significantly reduced breast cancer tumor growth (Figure 3B) and improved the survival of mice (Figure 3C). In addition, when AT3-OVA TILs were examined 2 weeks after dual-ICB therapy (Figure S3A), we observed a significantly increased number of endogenous $TCR\beta^+$ T cells (Figure S3B), and a significantly higher ratio of cytotoxic CD8:CD4 T cells, and CD8:$Foxp3^+CD4^+$ T_{reg} cells compared with control isotype-treated tumors (Figures S3C and S3D).

We next assessed the proportion of $CD69^+CD103^-$ and $CD103^+$ $CD8^+$ T cell populations in the MFP tumors following ICB therapy. Compared with the isotype-treated group, the blockade of both PD-1 and CTLA-4 resulted in a significant increase in the quantity of both intratumoral $CD69^+CD103^-$ and $CD103^+$ $CD8^+$ T cell populations (Figure 3D). We next examined the functional profile of the $CD69^+CD103^-$ and $CD69^+CD103^+$ T cells. The number of interferon (IFN)-γ and tumor necrosis factor (TNF)-α producing $CD69^+CD103^-$ and $CD69^+CD103^+$ T cells were significantly increased with the dual vs. single-agent blockade (Figure 3E), as were the number of OVA-specific $CD8^+$ T cells (Figures S3E and S3F).

To assess the cytotoxic capacity of $CD69^+CD103^-$ and $CD69^+CD103^+$ T cells in TNBC tumors, we isolated these T cell populations from ICB-treated mice and co-cultured T cells with chromium-labeled tumor cells for 24 h. Notably, we found that the $CD69^+CD103^+$ T cells isolated after dual-ICB therapy mediated significantly greater tumor killing compared with the $CD69^+CD103^-$ T cells at 24 h (Figure 3F), with no significant difference observed at 4 h (Figure S3G). Furthermore, significantly higher levels of IFN-γ and TNF-α were present in co-cultures that contained tumor cells and $CD69^+CD103^+$ compared with $CD69^+CD103^-$ T cells (Figures 3G and 3H). To further define the mechanism by which these $CD103^+CD8^+$ T cells mediate lysis of tumor cells, we isolated both $CD103^+$ and $CD103^-$ T cells from dual-ICB-treated mice and co-cultured these cells independently with chromium-labeled tumor cells in the presence of neutralizing antibodies against IFN-γ or TNF-α. We found that the neutralization of TNF-α or IFN-γ significantly reduced tumor cell lysis in both culture conditions compared with isotype-treated controls (Figure 3I). Together, these data support the superior cytotoxic potential of $CD69^+CD103^+$ T_{RM}-like cells compared with their $CD103^-$ T_{EX}-like counterparts.

(C) Percent survival of mice with tumor volume > 500 mm^3 post ICB with statistics shown on day 38, n = 10. Log rank (Mantel-Cox) test.
(D and E) TILs analyzed by FACS on day 28 post BC inoculation, for the differentiation of $CD69^+CD103^-$ (T_{EX}) and $CD69^+CD103^+$ (T_{RM}-like) cells among $CD44^{hi}CD8^+$ T cells.
(D) Total number of indicated T cell sub-populations among $CD44^{hi}CD8^+$ TILs per gram of tumor. Two-tailed Mann-Whitney test.
(E) Number of IFN-γ^+ and TNF-α^+ cytokine producing $CD8^+$ T cells among indicated phenotypes, mean ± SEM with n = 12 mice shown from two independent experiments. Two-tailed Mann-Whitney test.
(F–I) After two doses of anti-isotype (2A3), anti-PD-1, anti-CTLA-4, or dual-ICB treatment, tumor-infiltrating $CD69^+CD103^-$ (T_{EX}) and $CD69^+CD103^+$ (T_{RM}-like) $CD44^{hi}CD8^+$ T cells were FACS sorted and co-cultured with chromium[51] labeled AT3-OVA BC cells for 24 h.
(F) Percent specific lysis of AT3-OVA target cells after 24 h of co-culture with indicated $CD8^+$ T cell sub-populations (n = 3–4). Two-tailed Mann-Whitney test.
(G and H) Cell supernatants derived from indicated $CD8^+$ T cell sub-populations after 24 h were assessed for cytokines by cytometric bead array (CBA).
(G) Quantity of IFN-γ (pg/mL) (n = 3–4). Two-tailed Mann-Whitney test.
(H) Quantity of TNF-α (pg/mL) (n = 3–4). Two-tailed Mann-Whitney test.
(I) Percent specific lysis of AT3-OVA cells by $CD69^+CD103^-$ (T_{EX}) and $CD69^+CD103^+$ (T_{RM}-like) cells after dual-ICB therapy and co-cultured in the presence of indicated neutralizing antibodies. Mean ± SEM, each symbol represents an individual sample with averaged duplicates (n = 3–4). Two-tailed Mann-Whitney test.
(J) Percent mean expression of TCR-$V\beta^+$ clones indicated among indicated phenotypes on day 28 post ICB therapy. p values represent significantly increased TCR-Vβ clones relative to isotype controls. n = 4 mice shown from one of two independent experiments with similar results. Unpaired two-tailed Student's t test.
*$p < 0.05$; **$p < 0.01$; ****$p < 0.0001$, ns, not significant.
See also Figure S3 and Table S4.

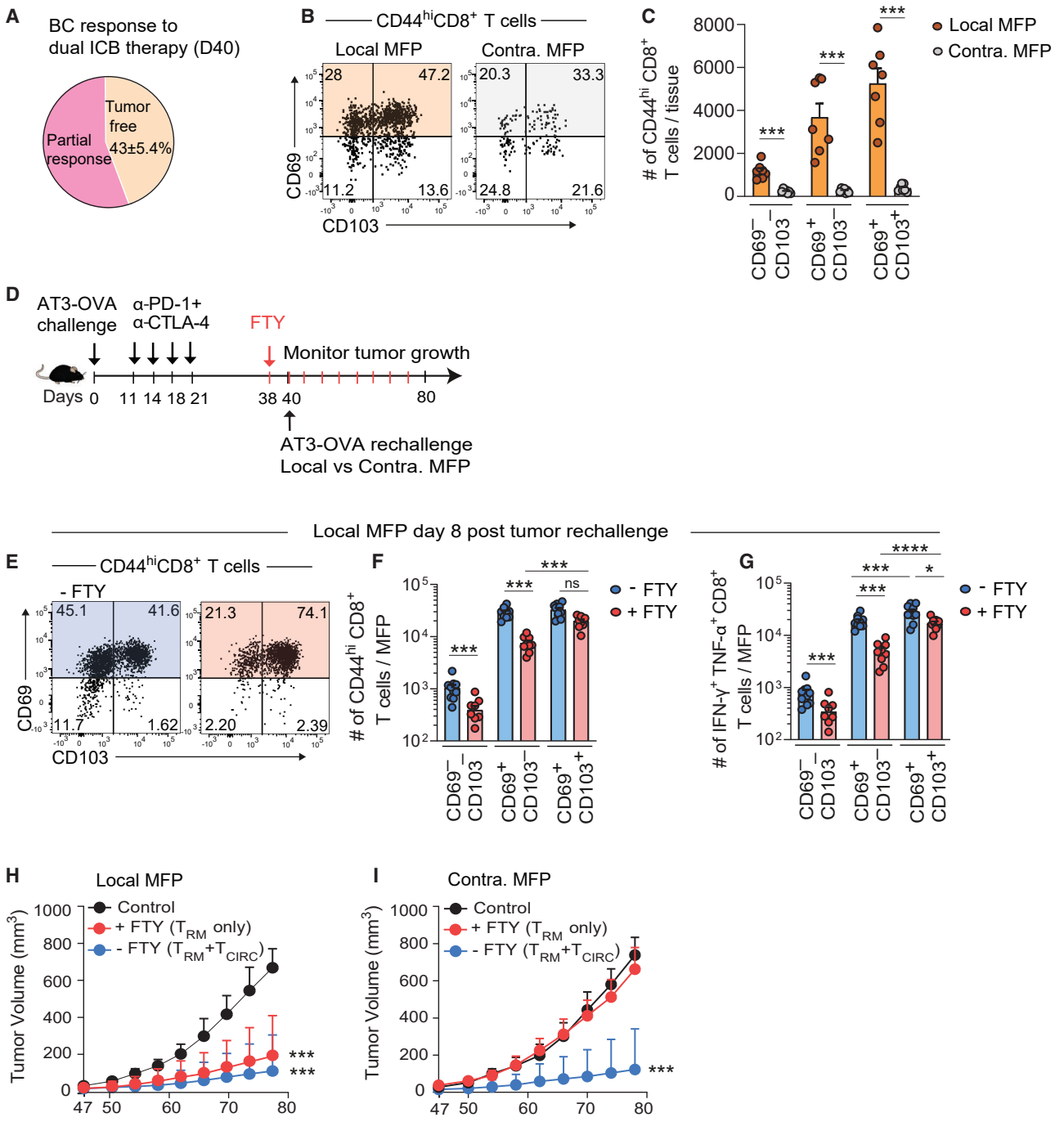

Figure 4. CD8⁺ T_{RM}-like cells confer local immune protection to TNBC tumor rechallenge

(A–C) AT3-OVA tumor-free local and naive contralateral MFP tissue post dual-ICB therapy on day 40 assessed for CD69⁻CD103⁻ (T_{CIRC}), CD69⁺CD103⁻ (T_{EX}), and CD69⁺CD103⁺ (T_{RM}-like) CD44^{hi}CD8⁺ TILs.

(A) Percentage of tumor-free mice (n = 76) pooled from three independent experiments.

(B) Representative CD69 and CD103 expression on CD8⁺ T cells in local MFP (left) and naive contralateral MFP (right).

(C) Total number of indicated T cell sub-populations among CD8⁺ T cells in local and naive contralateral MFP n = 7 shown from two independent experiments. Two-tailed Mann-Whitney test.

(D–I) Tumor-free mice post dual-ICB therapy were rechallenged with AT3-OVA BC cells in the local vs. contralateral MFP on day 40 in the presence or absence of FTY720 (FTY) treatment. (D) Schematic experimental design. (E–G) TILs were analyzed for CD69⁺CD103⁻ (T_{EX}) and CD69⁺CD103⁺ (T_{RM}-like) CD44^{hi}CD8⁺ T cells on day 8 post tumor rechallenge in the presence or absence of FTY. (E) Representative CD69 and CD103 expression on CD8⁺ T cells in local MFP. (F) Total number of CD69⁻CD103⁻ (T_{CIRC}), CD69⁺CD103⁻ (T_{EX}) and CD69⁺CD103⁺ (T_{RM}-like) cells among CD44^{hi}CD8⁺ T cells in the local MFP. Two-tailed Mann-Whitney test. (G) Total number of IFN-γ⁺ and TNF-α⁺ cytokine producing CD69⁻CD103⁻ (T_{CIRC}), CD69⁺CD103⁻ (T_{EX}), and CD69⁺CD103⁺ (T_{RM}-like) cells in the local MFP.

(legend continued on next page)

We next evaluated whether the quantitative increase of TIL following checkpoint therapy was also associated with clonal expansion of $CD8^+$ T cells in mammary tumors. The changes in the TCR repertoire in mammary tumors were evaluated by analysis of TCR-Vβ clonotypes at day 28 post tumor inoculation by using flow cytometry. As anticipated, a significant expansion of 9 of 14 Vβ clonotypes was observed in $CD69^+CD103^+$ T_{RM}-like cells (Figure 3J, right) and 8 of 14 Vβ clonotypes in $CD69^+CD103^-$ T cells in dual-ICB-treated relative to the isotype-treated cohort (Figure 3J, left). We observed that most significantly expanded TCR-Vβ clones (82% ± 6%) post ICB treatment were shared between the $CD69^+CD103^-$ and $CD69^+CD103^+$ T cells, unlike at week 2 post tumor inoculation (and pre-treatment) where the scTCR-aß clonotypes were different between the subsets of interest (Figure 2K). In addition, an assessment of TCR-Vβ clonotypes on $CD69^+CD103^-$ and $CD69^+CD103^+$ T cells revealed a significant expansion of OVA-specific tumor clones (Vβ5.1/5.2; Vβ8.1/8.2) with numerically more TCR-Vβ clones present post dual-ICB compared with the isotype control treated group (Figures S3H–S3K, Table S4). Overall, these data indicate that checkpoint blockade therapy resulted in TCR-Vβ clonal expansion and diversification, along with the increased production of TNF-α, IFN-γ, and killing capability resulting in superior anti-tumor activity of the $CD69^+CD103^+$ T cells. Given this, we hereafter refer to $CD69^+CD103^-$ and $CD69^+CD103^+$ T cell populations as $CD8^+$ T_{EX}-like and $CD8^+$ T_{RM}-like cells, respectively.

Local $CD8^+$ resident T cells in the MFP confer protection to secondary breast tumor rechallenge

Dual checkpoint inhibitor therapy with PD-1 and CTLA-4 in tumor-bearing mice resulted in 43% ± 5% mice being tumor-free at day 40 (Figure 4A) and 55% by day 65 (Figures S4A and S4B) and enhanced the survival of mice (Figure S4C). We examined for the persistence of both $CD8^+$ T cell sub-populations in the MFP of mice that had previously cleared their tumors following dual-ICB therapy. As expected, we found high numbers of $CD44^{hi}CD8^+$ T cells, comprising both $CD69^+CD103^-$ and $CD69^+CD103^+$ T cells compared with $CD69^-CD103^-$ circulating T cells, specifically within the previously inoculated MFP (local) compared with the contralateral MFP, consistent with the notion that these cells remain locally within tissues with minimal recirculation (Figures 4B and 4C). We next investigated the role of these T cells in the anti-tumor memory response by rechallenging the tumor-free mice with AT3-OVA cells in the local and naive contralateral tumor-free MFP at the day 40 timepoint post initial tumor inoculation. To determine the role for both local and circulating T cells in this memory response, we rechallenged mice in the presence or absence of FTY720 (Figure 4D). FTY720 blocks T cell trafficking and egress thereby enabling investigation of the importance of the localized immune response[24] (Figures S4D and S4E). Following secondary tumor challenge, we found significantly increased number of $CD69^+CD103^+$ T_{RM}-like cells in the local MFP of FTY720-treated mice compared with $CD69^+CD103^-$ T_{EX}-like and $CD69^-CD103^-$ T cells, confirming the resident nature of these $CD69^+CD103^+$ cells (Figures 4E, 4F, S4F, and S4G). In these FTY720-treated mice, we also observed significantly more IFN-γ and TNF-α production by $CD69^+CD103^+$ compared with $CD69^+CD103^-$ T cells (Figure 4G).

Importantly, in FTY720-treated mice, we observed significant secondary tumor protection, supporting the protective ability of the localized immune T_{RM} response without the need for the contribution of circulating memory T cells. We found that 7 of 14 (50% ± 10%) mice remained tumor-free in the local MFP up to 80 days from primary tumor inoculation (Figure 4H). In contrast, following inoculation of the contralateral MFP (which was comparatively devoid of $CD8^+$ T cells, Figure 4B), all mice within the FTY720-treated cohort developed secondary tumors (Figure 4I). Of note, we observed tumor protection in mice that were not treated with FTY720, in both local and contralateral MFP sites (Figures 4H and 4I), highlighting the important contribution of circulating memory T cells in ongoing breast cancer immunosurveillance at distal sites, presumably indicative of the generation of tumor-specific memory T cells that arise from the tumor and move into the circulation.

A gene signature from $CD69^+CD103^+CD8^+$ T_{RM}-like cells obtained from day 40 tumor-free mice is associated with benefit from ICB treatment in human cancers

We hypothesized that the gene expression profile of local T_{RM}-like cells remaining in the tumor-free MFP after dual-ICB therapy of mice at day 40 (D40) post tumor inoculation (Figure 4B) would be associated with improved clinical outcomes in patient cohorts, as these T_{RM}-like cells have remained in the absence of antigen, analogous to healthy tissue T_{RM} cells post pathogen clearance. The genes associated with $CD8^+$ T_{RM}-like cells on D40 are presented in Figure 5A (Table S5). This D40 $CD8^+$ T_{RM}-like gene signature had minimal overlap with previously published T_{RM} signatures from human TNBC and mouse T_{RM} cells (Figure S5A) and yet were highly correlated (R = 0.83; Figure S5B). Comparing $CD69^+CD103^+$ T_{RM} vs. $CD69^+CD103^-$ $CD8^+$ T_{EX} T cells at D40 revealed that the former was significantly enriched in genes similar to human melanoma T_{RM} cells vs. T_{EX} cells, respectively[64] (Figures 5B and 5C).

First, we examined the 329 cases of TNBC in the METABRIC cohort of early-stage breast cancers[65] (Figures 5D and 5E). These patients received a variety of treatments without immunotherapy. We found that higher expression of the D40 $CD8^+$ T_{RM} gene signature was significantly associated with improved prognosis in the TNBC cohort. We next examined the association between the D40 $CD8^+$ T_{RM} signature and pathological complete responses (pCR) in the ISPY clinical trial dataset of patients with early-stage breast cancers who received standard chemotherapy with or without a PD-1 inhibitor.[66] pCR refers to

n = 10 shown from two independent experiments. Two-tailed Mann-Whitney test. (H) Secondary tumor growth in the local MFP post tumor rechallenge. Two-way ANOVA with Tukey's multiple comparisons test. (I) Secondary tumor growth in contralateral (Contra.) MFP after tumor rechallenge, mean ± SEM with n = 14 in the FTY-treated group, n = 13 in the FTY untreated group, shown from two independent experiments. Each symbol represents an individual mouse. Two-way ANOVA with Tukey's multiple comparisons test. ***p < 0.001; ****p < 0.0001, ns, not significant.
See also Figure S4.

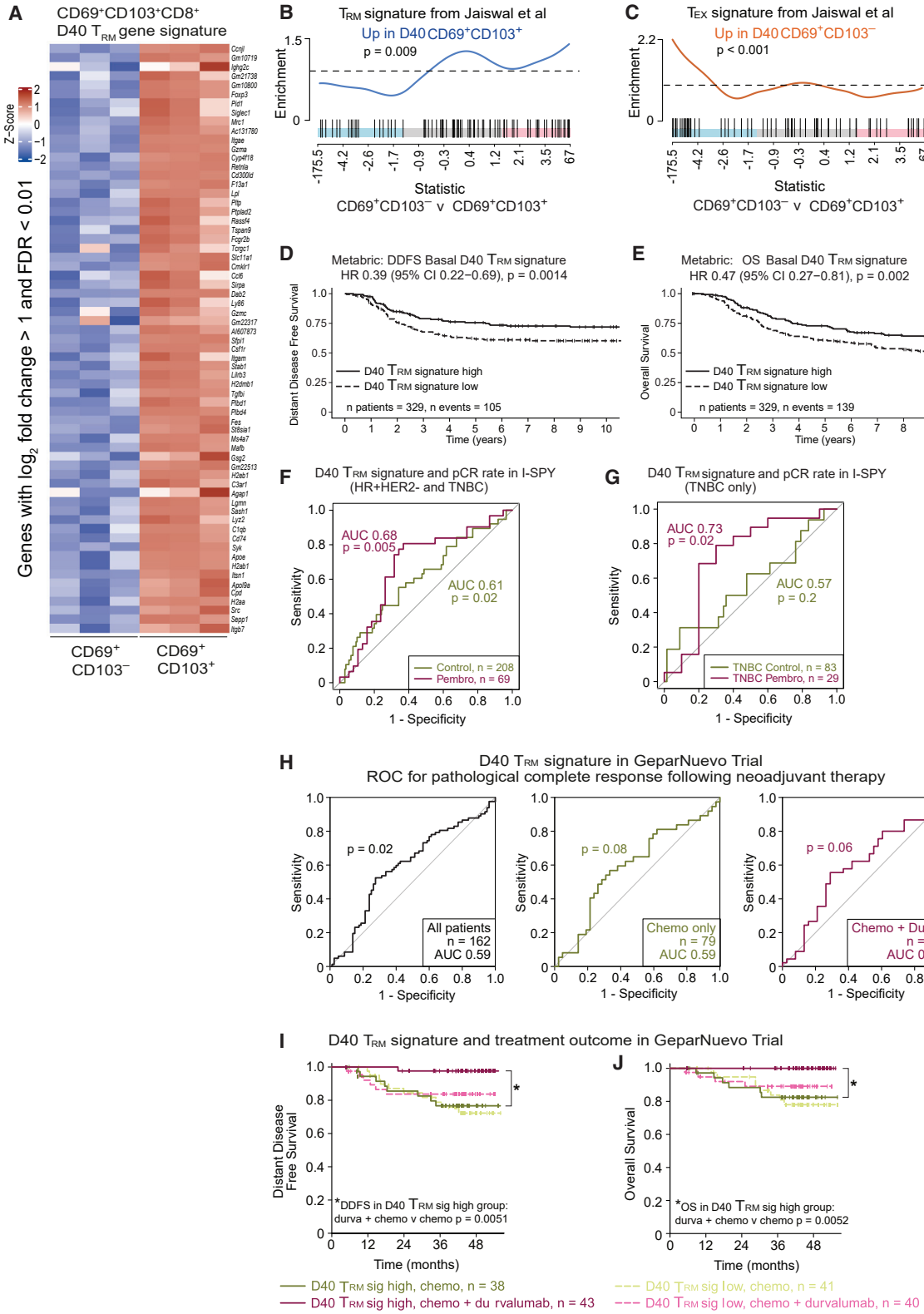

Figure 5. CD8$^+$ T_{RM} cell gene signature predicts patient clinical response to ICB therapy

(A) Heatmap of CD69$^+$CD103$^+$CD8$^+$ D40 T_{RM} signature genes upregulated CD69$^+$CD103$^+$ (T_{RM}-like) cells compared with CD69$^+$CD103$^-$ (T_{EX}) and. Genes with $\log_2$ fold change >1 and FDR <0.01 are shown ranked by fold change in descending order.

(legend continued on next page)

complete eradication of tumor cells in the breast and draining lymph nodes determined via histological review of surgical specimens, and is strongly associated with better distant disease-free and overall survival outcomes.[67] In the ISPY dataset, higher signature expression was associated with a higher chance of achieving a pCR in all HER2-negative breast cancers regardless of treatment (n = 277; Figure 5F). However, in patients with TNBC (n = 112), this association only held for those treated with pembrolizumab (Figure 5G). The GeparNeuvo phase II clinical trial randomized (n = 174) early-stage TNBC patients to receive standard chemotherapy with or without durvalumab (PD-L1 inhibitor).[43,68] Similar to the ISPY cohort, the D40 CD8$^+$ T_{RM} signature was associated with a higher rate of pCR (Figure 5H). However, more importantly, high expression was significantly associated with excellent survival outcomes with durvalumab compared with the chemotherapy alone arm, with almost no recurrences and no deaths in the patients who received durvalumab (p = 0.0051 for distant disease-free survival, p = 0.0052 for overall survival; Figures 5I and 5J). As this clinical trial dataset has long-term outcomes available and the patients were randomized to receive the immune checkpoint agent or not, these data provide strong support for our D40 gene set being specific to checkpoint blockade.

Finally, we examined two datasets of samples from patients with advanced melanoma treated with anti-PD-1 therapy in combination with ipilimumab, or with nivolumab after ipilimumab.[34,69] In both clinical datasets, the murine CD8$^+$ T_{RM}-like signature was significantly associated with improved objective responses (Figures S5C and S5D) and progression-free survival (Figures S5E and S5F), respectively. Overall, these data further solidify the critical role of resident CD8$^+$ T cells in the context of immune checkpoint blockade therapy, particularly for patients with early-stage TNBC, emphasizing the importance of the local immune response, the presence of T_{RM} cells in the breast tissue, as well as associations with better long-term survival after treatment with chemotherapy plus PD-1 therapy.

DISCUSSION

Treatment with immune checkpoint inhibitors can induce robust anti-tumor immune responses; however, this therapy only appears to benefit a subset of patients with solid cancers.[70] Patients with TNBC have only recently seen the incorporation of PD-1 immune checkpoint inhibitors with their standard chemotherapy despite the long-standing observation that higher TIL levels correlate with better clinical outcomes.[71–73] Several studies in human solid cancers, including our previous work in human TNBCs using scRNA-seq, have shown the presence of resident memory T cells in the tumoral immune infiltrate and their associations with improved outcomes.[12,14,36,74] Therefore, we hypothesized that immune checkpoint therapies target the local tumor microenvironment and that the CD8$^+$ T_{RM} cells could be critical for their efficacy in breast cancer. We here demonstrate that intratumoral CD8$^+$ T cells, particularly those with a resident phenotype, contribute to breast cancer anti-tumor responses as well as their role in ongoing breast cancer protective immunity in a murine model of TNBC.

In this work, we establish the phenotypic characteristics and cytokine requirements for generation and maintenance of distinct intratumoral CD8$^+$ T cell sub-populations in breast cancer. With regard to the relationship between the CD69$^+$CD103$^+$ and CD69$^+$CD103$^-$ subsets, we have previously shown that while CD69$^+$CD103$^-$ can differentiate into CD103$^+$ cells (and other memory populations) in the setting of acute viral infection, the CD103$^+$ population comparatively resists de-differentiation and appears to have a fixed cell fate.[75] We further confirm molecular differences in these intratumoral populations, demonstrating that the CD69$^+$CD103$^-$ subset displays elevated expression of T_{EX}-associated genes such as *Tox* and *Eomes*,[76] and display a transcriptional profile similar to terminally exhausted T cells in the context of chronic lymphocytic choriomeningitis virus (LCMV).[61,62] In contrast, the CD69$^+$CD103$^+$ subset demonstrated enhanced anti-tumor function (in terms of cytotoxicity and inflammatory cytokine secretion) in mediating tumor lysis. These T cell sub-populations were further validated by unbiased clustering of CD8$^+$ single-cell transcriptomic data analyzed pre ICB treatment. Two clusters, distinguished by expression of *Itgae* and *Tox*, bore significant transcriptional similarities to bulk RNA-seq of sorted CD69$^+$CD103$^+$ and CD103$^-$ subsets, respectively. In addition, these support the use of CD103 and CD69 markers to define our subsets of interest. It is also important to note that while CD69$^+$CD103$^-$ cells in established tumors display T_{EX}-like features, in the context of checkpoint blockade or tumor rechallenge, the CD69$^+$CD103$^-$ population will likely become highly heterogeneous. In these contexts, cells classified

(B and C) GSEA of CD69$^+$CD103$^-$ vs. CD69$^+$CD103$^+$ CD44^{hi}CD8$^+$ T cell populations isolated from local MFP tissue of tumor free mice on day 40 (D40) post tumor inoculation. (B) Significant enrichment of core T_{RM} gene signature[64] in D40 CD69$^+$CD103$^+$ compared with CD69$^+$CD103$^-$ CD8$^+$ T cell phenotype. (C) Significant enrichment of genes associated with "T cell exhaustion signature" derived from melanoma CD8$^+$ TIL dataset[64] in D40 CD69$^+$CD103$^-$ CD8$^+$ T_{EX} population. Human homologs are used for the following human survival analyses, see Table S5.

(D) Kaplan-Meier survival curves for distant disease-free survival.

(E) Overall survival from n = 329 primary basal-like/TNBCs showing significant prognostic separation according to D40 T_{RM} gene signature with hazard ratio and p value log rank test.

(F–H) Receiver operating characteristic (ROC) plots and area under the curve (AUC) scores were assessed.

(F) Performance of the D40 CD8$^+$ T_{RM} signature to predict pathological complete response (pCR) in HER2- BC patients treated with (anti-PD-1) pembrolizumab plus chemotherapy. (G) Performance of the D40 T_{RM} signature to predict pCR specifically in TNBC patients treated with pembrolizumab plus chemotherapy compared with control treatment group in I-SPY2-990 dataset. (H) ROC curves indicating performance of D40 T_{RM} gene signature to significantly predict pCR following neoadjuvant therapy in all patients (n = 162), chemotherapy treated (n = 79), and chemotherapy + durvalumab (n = 83) treated patients from randomized phase II GeparNuevo clinical trial in early-stage triple-negative breast cancer.

(I) Kaplan-Meier survival curves with distant disease-free survival and (J) overall survival from GeparNuevo trial. Patients in each treatment arm stratified based on D40 T_{RM} signature, p value log rank test demonstrating D40 T_{RM} signature is specific for treatment with durvalumab.

See also Figure S5 and Table S5.

as CD69$^+$CD103$^-$ will include newly infiltrated effector cells and precursor memory cells, in addition to those with T_{EX}-like features. Thus, it is possible in this context that CD69$^+$CD103$^-$ cells may also give rise to CD69$^+$CD103$^+$ T cells following local inflammatory signals including TGF-β, within the breast tumor microenvironment.

PD-1/PD-L1 checkpoint inhibitors in combination with chemotherapy have only recently been shown to be efficacious for patients with TNBC.[72,73] In patients with advanced disease, pre-existing PD-L1-positive immune cells are essential for response to these agents.[39,77] Our data are consistent with a previous study in melanoma-bearing mice where PD-1 blockade resulted in a 10-fold increase in T_{RM} formation following T_{CM} transfer and that this was associated with superior anti-tumor efficacy *in vivo*.[22] Correlative studies in human oral cancer and melanoma also report an association between increases in T cells with residency features and better clinical responses to immune checkpoint blockade.[18,78] Progenitor exhausted T cells (T_{PEX}) have also been shown to proliferate in tumor-draining lymph nodes in response to PD-1 blockade.[79] We also noted the presence of a small *Tcf7*$^+$ (TCF1$^+$) expressing cluster in our single-cell data. Our work is not inconsistent with this literature; however, here we show the importance of the local intratumoral T cell populations, especially the T_{RM} subtype in mediating checkpoint inhibitor efficacy. Future work will likely delineate the relationship between T_{PEX} cells and if they can differentiate into intratumoral T_{RM} populations post checkpoint inhibitor therapy.

Of high importance are our findings underlining the significance of CD8$^+$ T_{RM}-like cells in ongoing breast cancer immune surveillance, particularly post-immune checkpoint blockade. Notably the T_{RM}-like cells remaining in the MFP post tumor clearance could expand locally and protect from secondary tumor rechallenge with a minimal role for circulating T cells. In contrast, the tumor-naïve MFP distal to site of the primary tumor lacked T_{RM} cells and required circulating T cells for immune protection from tumor growth. These data provide support for the hypothesis that tumor-specific memory T cells can be generated and mobilized from the tumor to protect against distant metastases formation as suggested by Luoma et al.[78] Our work, now in breast cancer, supports previous published reports in melanoma that indicates that pre-existing CD8$^+$ T_{RM}-like cells can be sufficient to independently confer tissue immune protection following rechallenge.[23,24]

It is likely that immune checkpoint blockade induces both a local and systemic immune response that protects against formation of distant metastases in patients. We therefore show the clinical relevance of our findings by developing a transcriptional profile of the T_{RM}-like cells that persisted in the MFP of tumor-free mice at D40 post tumor inoculation. We chose this time point to profile as we hypothesized that these cells could be more analogous to pathogen-induced CD8$^+$ T_{RM} cells that subsequently survive in the absence of antigen and mediate local tissue defense. We show the prognostic significance of this signature in the METABRIC TNBC dataset, with an effect size of similar magnitude to a gene set we published previously.[13] Despite minimal overlap in genes between this scRNA-seq signature derived from human CD3$^+$ T cells and the current gene set derived from a murine model, it is notable that the current signature can have similar prognostic value.

Combined PD-1 inhibition plus chemotherapy is now a US Food and Drug Administration-approved standard of care neoadjuvant therapy for early-stage TNBC. This approval followed the KEYNOTE-522 phase 3 trial demonstrating higher pathological complete response (pCR) rates and improved event-free survival over chemotherapy alone.[41] To understand the clinical relevance of tissue-resident immunity to checkpoint inhibition, we show that our murine T_{RM}-like signature is significantly associated with pCR after treatment of early-stage breast cancer with neoadjuvant chemotherapy with and without a PD-L1 inhibitor. A recent intriguing finding is that neoadjuvant PD-1 inhibition combined with chemotherapy dramatically improves survival over chemotherapy alone even in patients in whom pCR is not achieved.[68,80] We therefore used the GeparNuevo randomized clinical trial to explore the prognostic significance of our signature beyond pCR rates and found that PD-L1 inhibition plus chemotherapy produced near complete freedom from recurrence in tumors with high signature expression. This benefit was not seen with chemotherapy alone without PD-L1 inhibition and high tumor signature expression. Although this result requires replication in other clinical trial cohorts with mature survival outcome data, it provides strong evidence for the clinical relevance of our findings, supporting the importance of tissue-resident memory T cells in ICB treatment as it is currently delivered in the clinic, influencing both local and distant disease control in breast cancer patients. Our findings indicate that tissue-resident adaptive immunity contributes significantly to the enhanced tumor eradication seen in patients with TNBC treated with checkpoint inhibition in combination with chemotherapy.

In summary, we demonstrate the tissue residence and functional properties of the CD69$^+$CD103$^+$CD8$^+$ T_{RM}-like cells in TNBC and establish the critical contribution of local resident CD8$^+$ T cells in checkpoint blockade responses and ongoing breast cancer protective immunity. Our data are further supported by transcriptional profile from T_{RM} cells derived from tumor-free MFP and its significant associations with clinical outcomes in datasets of patients with TNBC treated with chemotherapy and checkpoint inhibition. We conclude that approaches to identify, induce, and amplify CD8$^+$ T_{RM} cells will be advantageous for the development of successful future immunotherapies in breast and likely other solid cancers.

STAR★METHODS

Detailed methods are provided in the online version of this paper and include the following:

- KEY RESOURCES TABLE
- RESOURCE AVAILABILITY
  - Lead contact
  - Materials availability
  - Data and code availability
- EXPERIMENTAL MODEL AND SUBJECT DETAILS
  - Mouse cell lines
  - Mouse models
  - Human studies
- METHOD DETAILS
  - Adoptive transfer of transgenic CD8$^+$ T cells
  - Treatment of tumor bearing mice

- FACS analysis of TILs
- Intracellular cytokine staining
- Chromium release assay
- Cytometric bead array
- Gene expression analysis
- ScRNA-seq of FACS sorted T cells
- Gene set enrichment analysis
- Survival cohort analyses

● QUANTIFICATION AND STATISTICAL ANALYSIS

SUPPLEMENTAL INFORMATION

Supplemental information can be found online at https://doi.org/10.1016/j.ccell.2023.01.004.

ACKNOWLEDGMENTS

The authors acknowledge staff from the Peter MacCallum Cancer Center Flow Facility, Peter MacCallum Molecular Genomics core and Peter MacCallum Cancer Center Animal Research Platform, and the Australian genome research facility (AGRF, Melbourne) for their assistance. Graphical abstract was created with BioRender.com. We thank Jeannette Parrodi for administrative support.

S.Loi. is supported by the National Breast Cancer Foundation of Australia (NBCF) (APP ID: EC-17-001), the Breast Cancer Research Foundation, New York (BCRF (APP ID: BCRF-21-102), and a National Health and Medical Council of Australia (NHMRC) Investigator Grant (APP ID: 1162318).

L.K.M. is supported by the Grant-In-Aid Scheme administered by Cancer Council Victoria.

P.K.D. is supported by a National Health and Medical Research Council Principal Research Fellowship (APP ID: 1136680). C.S. is a Royal Society Napier Research Professor (RSRP\R\210001).

C.S. is a Royal Society Napier Research Professor (RSRP\R\210001). His work is supported by the Francis Crick Institute that receives its core funding from Cancer Research UK (CC2041), the UK Medical Research Council (CC2041), and the Wellcome Trust (CC2041) and the Breast Cancer Research Foundation (US) BCRF-22-157. For the purpose of Open Access, the author has applied a CC BY public copyright licence to any Author Accepted Manuscript version arising from this submission.C.D., and S.Loibl are supported by a research grant from the German Cancer Aid (Deutsche Krebshilfe, Translational Oncology, Integrate-TN project; 70113450) and European Commission H2020 (Oncobiome project; 825410).

AUTHOR CONTRIBUTIONS

B.V. performed the experiments, analyzed results, coordinated the project, and wrote the research manuscript. F.C., P.S., S.S., and S.N.C. supported with interpretation of results, performed experiments, analyzed results, and reviewed the manuscript. F.C., P.S., J.W., T.P.S., and L.C.G. generated programming scripts and analyzed the bioinformatics results. A.B., K.C., E.B., B.V.S., D.F., K.W., J.T.S, C.D., S. Loibl, O.L., C.S., R.L., S.J.L., and Z.L.T. supported with experiments. P.J.N. and P.K.D., L.K.M., and S. Loi. conceived the project, directed provided scientific expertise, and approved the final research manuscript. S. Loi., as leading senior author, conceived the project, coordinated the project, and provided the project funding.

DECLARATION OF INTERESTS

P.S. receives research funding from Roche-Genentech. S.Loi receives research funding to her institution from Novartis, Bristol-Meyers Squibb, Merck, Puma Biotechnology, Eli Lilly, Nektar Therapeutics, Astra Zeneca, Roche-Genentech, and Seattle Genetics. S.Loi has acted as consultant (not compensated) to Seattle Genetics, Novartis, Bristol-Meyers Squibb, Merck, AstraZeneca, Eli Lilly, Pfizer, and Roche-Genentech. S.Loi has acted as consultant (paid to her institution) to Aduro Biotech, Novartis, GlaxoSmithKline, Roche-Genentech, Astra Zeneca, Silverback Therapeutics, G1 Therapeutics, PUMA Biotechnologies, Pfizer, Gilead Therapeutics, Seattle Genetics, Daiichi-Sankyo, Amunix, Tallac Therapeutics, Eli Lilly, and Bristol-Meyers. S. Loi has filed a provisional patent application in Australia based on methods for patient stratification described in this manuscript. Squibb. P.K.D. receives research funding from Myeloid Therapeutics, Prescient Therapeutics, and Bristol-Myers Squibb. S.Loibl reports grants and other from Abbvie; other from Amgen; grants and other from AstraZeneca; other from BMS; grants and other from Celgene; grants, non-financial support, and other from Daiichi-Sankyo; other from Eirgenix; other from Eisai Europe Ltd; other from GSK; grants, non-financial support, and other from Immunomedics/Gilead; other from Lilly; other from Merck; grants from Molecular Health; grants, non-financial support, and other from Novartis; grants, non-financial support, and other from Pfizer; other from Pierre Fabre; other from Relay Therapeutics; grants, non-financial support, and other from Roche; other from Sanofi; non-financial support and other from Seagen, outside the submitted work. In addition, S.Loibl has a patent EP14153692.0 pending, a patent EP21152186.9 pending, a patent P15702464.7 issued, a patent EP19808852.8 pending, and a patent Digital Ki67 Evaluator with royalties paid. C.S. acknowledges grant support from AstraZeneca, Boehringer-Ingelheim, Bristol-Myers Squibb, Pfizer, Roche-Ventana, Invitae (previously Archer Dx Inc - collaboration in minimal residual disease sequencing technologies), and Ono Pharmaceutical. He is an AstraZeneca Advisory Board member and Chief Investigator for the AZ MeRmaiD 1 and 2 clinical trials and is Co-Chief Investigator of the NHS Galleri trial funded by GRAIL and a paid member of GRAIL's Scientific Advisory Board. He receives consultant fees from Achilles Therapeutics (also SAB member), Bicycle Therapeutics (also a SAB member), Genentech, Medicxi, Roche Innovation Center – Shanghai, Metabomed (until July 2022), and the Sarah Canon Research Institute. C.S has received honoraria from Amgen, AstraZeneca, Pfizer, Novartis, GlaxoSmithKline, MSD, Bristol-Myers Squibb, Illumina, and Roche-Ventana. C.S. had stock options in Apogen Biotechnologies and GRAIL until June 2021, and currently has stock options in Epic Bioscience, Bicycle Therapeutics, and has stock options and is co-founder of Achilles Therapeutics. C.S. holds patents relating to assay technology to detect tumor recurrence (PCT/GB2017/053289); to targeting neoantigens (PCT/EP2016/059401), identifying patent response to immune checkpoint blockade (PCT/EP2016/071471), determining HLA LOH (PCT/GB2018/052004), predicting survival rates of patients with cancer (PCT/GB2020/050221), identifying patients who respond to cancer treatment (PCT/GB2018/051912), US patent relating to detecting tumor mutations (PCT/US2017/28013), methods for lung cancer detection (US20190106751A1) and both a European and US patent related to identifying insertion/deletion mutation targets (PCT/GB2018/051892).

C.D. reports grants from European Commission H2020, grants from German Cancer Aid Translational Oncology, grants from German Breast Group, during the conduct of the study; personal fees from Novartis, Roche, MSD Oncology, Daiichi Sankyo, AstraZeneca, Merck, Molecular Health, grants from Myriad and Roche to the institution, grants from GBG foundation to the institution, other from Sividon diagnostics, outside the submitted work; In addition, Dr. Denkert has a patent on VMscope digital pathology software with royalties paid, a patent WO2020109570A1 - cancer immunotherapy pending, and a patent WO2015114146A1 and WO2010076322A1- therapy response issued.A provisional patent application has been filed in Australia based on methods for patient stratification disclosed in this manuscript.

INCLUSION AND DIVERSITY

We support inclusive, diverse, and equitable conduct of research.

Received: May 4, 2022
Revised: October 17, 2022
Accepted: January 13, 2023
Published: February 23, 2023

REFERENCES

1. Ariotti, S., Beltman, J.B., Chodaczek, G., Hoekstra, M.E., van Beek, A.E., Gomez-Eerland, R., Ritsma, L., van Rheenen, J., Marée, A.F.M., Zal, T., et al. (2012). Tissue-resident memory CD8+ T cells continuously patrol skin epithelia to quickly recognize local antigen. Proc. Natl. Acad. Sci. USA *109*, 19739–19744. https://doi.org/10.1073/pnas.1208927109.

2. Jiang, X., Clark, R.A., Liu, L., Wagers, A.J., Fuhlbrigge, R.C., and Kupper, T.S. (2012). Skin infection generates non-migratory memory CD8+ T(RM) cells providing global skin immunity. Nature *483*, 227–231. https://doi.org/10.1038/nature10851.

3. Mackay, L.K., Rahimpour, A., Ma, J.Z., Collins, N., Stock, A.T., Hafon, M.L., Vega-Ramos, J., Lauzurica, P., Mueller, S.N., Stefanovic, T., et al. (2013). The developmental pathway for CD103(+)CD8+ tissue-resident memory T cells of skin. Nat. Immunol. *14*, 1294–1301. https://doi.org/10.1038/ni.2744.

4. Schenkel, J.M., and Masopust, D. (2014). Tissue-resident memory T cells. Immunity *41*, 886–897. https://doi.org/10.1016/j.immuni.2014.12.007.

5. Gebhardt, T., Wakim, L.M., Eidsmo, L., Reading, P.C., Heath, W.R., and Carbone, F.R. (2009). Memory T cells in nonlymphoid tissue that provide enhanced local immunity during infection with herpes simplex virus. Nat. Immunol. *10*, 524–530. https://doi.org/10.1038/ni.1718.

6. Masopust, D., Choo, D., Vezys, V., Wherry, E.J., Duraiswamy, J., Akondy, R., Wang, J., Casey, K.A., Barber, D.L., Kawamura, K.S., et al. (2010). Dynamic T cell migration program provides resident memory within intestinal epithelium. J. Exp. Med. *207*, 553–564. https://doi.org/10.1084/jem.20090858.

7. Masopust, D., and Soerens, A.G. (2019). Tissue-resident T cells and other resident leukocytes. Annu. Rev. Immunol. *37*, 521–546. https://doi.org/10.1146/annurev-immunol-042617-053214.

8. Mueller, S.N., and Mackay, L.K. (2016). Tissue-resident memory T cells: local specialists in immune defence. Nat. Rev. Immunol. *16*, 79–89. https://doi.org/10.1038/nri.2015.3.

9. Gebhardt, T., Whitney, P.G., Zaid, A., Mackay, L.K., Brooks, A.G., Heath, W.R., Carbone, F.R., and Mueller, S.N. (2011). Different patterns of peripheral migration by memory CD4+ and CD8+ T cells. Nature *477*, 216–219. https://doi.org/10.1038/nature10339.

10. Mackay, L.K., Stock, A.T., Ma, J.Z., Jones, C.M., Kent, S.J., Mueller, S.N., Heath, W.R., Carbone, F.R., and Gebhardt, T. (2012). Long-lived epithelial immunity by tissue-resident memory T (TRM) cells in the absence of persisting local antigen presentation. Proc. Natl. Acad. Sci. USA *109*, 7037–7042.

11. Djenidi, F., Adam, J., Goubar, A., Durgeau, A., Meurice, G., de Montpréville, V., Validire, P., Besse, B., and Mami-Chouaib, F. (2015). CD8+CD103+ tumor-infiltrating lymphocytes are tumor-specific tissue-resident memory T cells and a prognostic factor for survival in lung cancer patients. J. Immunol. *194*, 3475–3486. https://doi.org/10.4049/jimmunol.1402711.

12. Boddupalli, C.S., Bar, N., Kadaveru, K., Krauthammer, M., Pornputtapong, N., Mai, Z., Ariyan, S., Narayan, D., Kluger, H., Deng, Y., et al. (2016). Interlesional diversity of T cell receptors in melanoma with immune checkpoints enriched in tissue-resident memory T cells. JCI Insight *1*, e88955. https://doi.org/10.1172/jci.insight.88955.

13. Savas, P., Virassamy, B., Ye, C., Salim, A., Mintoff, C.P., Caramia, F., Salgado, R., Byrne, D.J., Teo, Z.L., Dushyanthen, S., et al. (2018). Single-cell profiling of breast cancer T cells reveals a tissue-resident memory subset associated with improved prognosis. Nat. Med. *24*, 986–993. https://doi.org/10.1038/s41591-018-0078-7.

14. Ganesan, A.P., Clarke, J., Wood, O., Garrido-Martin, E.M., Chee, S.J., Mellows, T., Samaniego-Castruita, D., Singh, D., Seumois, G., Alzetani, A., et al. (2017). Tissue-resident memory features are linked to the magnitude of cytotoxic T cell responses in human lung cancer. Nat. Immunol. *18*, 940–950. https://doi.org/10.1038/ni.3775.

15. Duhen, T., Duhen, R., Montler, R., Moses, J., Moudgil, T., de Miranda, N.F., Goodall, C.P., Blair, T.C., Fox, B.A., McDermott, J.E., et al. (2018). Co-expression of CD39 and CD103 identifies tumor-reactive CD8 T cells in human solid tumors. Nat. Commun. *9*, 2724. https://doi.org/10.1038/s41467-018-05072-0.

16. Webb, J.R., Milne, K., Watson, P., deLeeuw, R.J., and Nelson, B.H. (2014). Tumor-infiltrating lymphocytes expressing the tissue resident memory marker CD103 are associated with increased survival in high-grade serous Ovarian cancer. Clin. Cancer Res. *20*, 434–444. https://doi.org/10.1158/1078-0432.CCR-13-1877.

17. Workel, H.H., Komdeur, F.L., Wouters, M.C., Plat, A., Klip, H.G., Eggink, F.A., Wisman, G.B., Arts, H.J., Oonk, M.H., Mourits, M.J., et al. (2016). CD103 defines intraepithelial CD8+ PD1+ tumour-infiltrating lymphocytes of prognostic significance in endometrial adenocarcinoma. Eur. J. Cancer *60*, 1–11. https://doi.org/10.1016/j.ejca.2016.02.026.

18. Edwards, J., Wilmott, J.S., M3adore, J., Gide, T.N., Quek, C., Tasker, A., Ferguson, A., Chen, J., Hewavisenti, R., Hersey, P., et al. (2018). CD103^{+} tumor-resident CD8^{+} T cells are associated with improved survival in immunotherapy-naïve melanoma patients and expand significantly during anti–PD-1 treatment. Clin. Cancer Res. *24*, 3036–3045. https://doi.org/10.1158/1078-0432.CCR-17-2257.

19. Hartana, C.A., Ahlén Bergman, E., Broomé, A., Berglund, S., Johansson, M., Alamdari, F., Jakubczyk, T., Huge, Y., Aljabery, F., Palmqvist, K., et al. (2018). Tissue-resident memory T cells are epigenetically cytotoxic with signs of exhaustion in human urinary bladder cancer. Clin. Exp. Immunol. *194*, 39–53. https://doi.org/10.1111/cei.13183.

20. Komdeur, F.L., Prins, T.M., van de Wall, S., Plat, A., Wisman, G.B.A., Hollema, H., Daemen, T., Church, D.N., de Bruyn, M., and Nijman, H.W. (2017). CD103+ tumor-infiltrating lymphocytes are tumor-reactive intraepithelial CD8+ T cells associated with prognostic benefit and therapy response in cervical cancer. OncoImmunology *6*, e1338230. https://doi.org/10.1080/2162402x.2017.1338230.

21. Wang, B., Wu, S., Zeng, H., Liu, Z., Dong, W., He, W., Chen, X., Dong, X., Zheng, L., Lin, T., and Huang, J. (2015). CD103+ tumor infiltrating lymphocytes predict a favorable prognosis in urothelial cell carcinoma of the bladder. J. Urol. *194*, 556–562. https://doi.org/10.1016/j.juro.2015.02.2941.

22. Enamorado, M., Iborra, S., Priego, E., Cueto, F.J., Quintana, J.A., Martínez-Cano, S., Mejías-Pérez, E., Esteban, M., Melero, I., Hidalgo, A., and Sancho, D. (2017). Enhanced anti-tumour immunity requires the interplay between resident and circulating memory CD8+ T cells. Nat. Commun. *8*, 16073. https://doi.org/10.1038/ncomms16073.

23. Malik, B.T., Byrne, K.T., Vella, J.L., Zhang, P., Shabaneh, T.B., Steinberg, S.M., Molodtsov, A.K., Bowers, J.S., Angeles, C.V., Paulos, C.M., et al. (2017). Resident memory T cells in the skin mediate durable immunity to melanoma. Sci. Immunol. *2*, eaam6346. https://doi.org/10.1126/sciimmunol.aam6346.

24. Park, S.L., Buzzai, A., Rautela, J., Hor, J.L., Hochheiser, K., Effern, M., McBain, N., Wagner, T., Edwards, J., McConville, R., et al. (2019). Tissue-resident memory CD8+ T cells promote melanoma–immune equilibrium in skin. Nature *565*, 366–371. https://doi.org/10.1038/s41586-018-0812-9.

25. Bianchini, G., Balko, J.M., Mayer, I.A., Sanders, M.E., and Gianni, L. (2016). Triple-negative breast cancer: challenges and opportunities of a heterogeneous disease. Nat. Rev. Clin. Oncol. *13*, 674–690. https://doi.org/10.1038/nrclinonc.2016.66.

26. Sharma, P. (2016). Biology and management of patients with triple-negative breast cancer. Oncol. *21*, 1050–1062. https://doi.org/10.1634/theoncologist.2016-0067.

27. Emens, L.A., Molinero, L., Loi, S., Rugo, H.S., Schneeweiss, A., Diéras, V., Iwata, H., Barrios, C.H., Nechaeva, M., Nguyen-Duc, A., et al. (2021). Atezolizumab and nab-paclitaxel in advanced triple-negative breast cancer: biomarker evaluation of the IMpassion130 study. J. Natl. Cancer Inst. *113*, 1005–1016. https://doi.org/10.1093/jnci/djab004.

28. Loi, S., Drubay, D., Adams, S., Pruneri, G., Francis, P.A., Lacroix-Triki, M., Joensuu, H., Dieci, M.V., Badve, S., Demaria, S., et al. (2019). Tumor-infiltrating lymphocytes and prognosis: a pooled individual patient analysis of early-stage triple-negative breast cancers. J. Clin. Oncol. *37*, 559–569. https://doi.org/10.1200/JCO.18.01010.

29. Ruffell, B., Au, A., Rugo, H.S., Esserman, L.J., Hwang, E.S., and Coussens, L.M. (2012). Leukocyte composition of human breast cancer. Proc. Natl. Acad. Sci. USA *109*, 2796–2801. https://doi.org/10.1073/pnas.1104303108.

30. König, L., Mairinger, F.D., Hoffmann, O., Bittner, A.-K., Schmid, K.W., Kimmig, R., Kasimir-Bauer, S., and Bankfalvi, A. (2019). Dissimilar patterns of tumor-infiltrating immune cells at the invasive tumor front and tumor center are associated with response to neoadjuvant chemotherapy in primary breast cancer. BMC Cancer *19*, 120. https://doi.org/10.1186/s12885-019-5320-2.

31. Byrne, A., Savas, P., Sant, S., Li, R., Virassamy, B., Luen, S.J., Beavis, P.A., Mackay, L.K., Neeson, P.J., and Loi, S. (2020). Tissue-resident memory T cells in breast cancer control and immunotherapy responses. Nat. Rev. Clin. Oncol. *17*, 341–348. https://doi.org/10.1038/s41571-020-0333-y.

32. Robert, C. (2020). A decade of immune-checkpoint inhibitors in cancer therapy. Nat. Commun. *11*, 3801. https://doi.org/10.1038/s41467-020-17670-y.

33. Wei, S.C., Anang, N.A.A.S., Sharma, R., Andrews, M.C., Reuben, A., Levine, J.H., Cogdill, A.P., Mancuso, J.J., Wargo, J.A., Pe'er, D., and Allison, J.P. (2019). Combination anti-CTLA-4 plus anti-PD-1 checkpoint blockade utilizes cellular mechanisms partially distinct from monotherapies. Proc. Natl. Acad. Sci. USA *116*, 22699–22709. https://doi.org/10.1073/pnas.1821218116.

34. Gide, T.N., Quek, C., Menzies, A.M., Tasker, A.T., Shang, P., Holst, J., Madore, J., Lim, S.Y., Velickovic, R., Wongchenko, M., et al. (2019). Distinct immune cell populations define response to anti-PD-1 monotherapy and anti-PD-1/anti-CTLA-4 combined therapy. Cancer Cell *35*, 238–255.e6. https://doi.org/10.1016/j.ccell.2019.01.003.

35. Tumeh, P.C., Harview, C.L., Yearley, J.H., Shintaku, I.P., Taylor, E.J.M., Robert, L., Chmielowski, B., Spasic, M., Henry, G., Ciobanu, V., et al. (2014). PD-1 blockade induces responses by inhibiting adaptive immune resistance. Nature *515*, 568–571. https://doi.org/10.1038/nature13954.

36. Corgnac, S., Malenica, I., Mezquita, L., Auclin, E., Voilin, E., Kacher, J., Halse, H., Grynszpan, L., Signolle, N., Dayris, T., et al. (2020). CD103(+) CD8(+) TRM cells accumulate in tumors of anti-PD-1-responder lung cancer patients and are tumor-reactive lymphocytes enriched with Tc17. Cell Rep. Med. *1*, 100127. https://doi.org/10.1016/j.xcrm.2020.100127.

37. Li, F., Li, C., Cai, X., Xie, Z., Zhou, L., Cheng, B., Zhong, R., Xiong, S., Li, J., Chen, Z., et al. (2021). The association between CD8+ tumor-infiltrating lymphocytes and the clinical outcome of cancer immunotherapy: a systematic review and meta-analysis. EClinicalMedicine *41*, 101134. https://doi.org/10.1016/j.eclinm.2021.101134.

38. Cho, J.-W., Park, S., Kim, G., Han, H., Shim, H.S., Shin, S., Bae, Y.-S., Park, S.Y., Ha, S.-J., Lee, I., and Kim, H.R. (2021). Dysregulation of TFH-B-TRM lymphocyte cooperation is associated with unfavorable anti-PD-1 responses in EGFR-mutant lung cancer. Nat. Commun. *12*, 6068. https://doi.org/10.1038/s41467-021-26362-0.

39. Adams, S., Schmid, P., Rugo, H.S., Winer, E.P., Loirat, D., Awada, A., Cescon, D.W., Iwata, H., Campone, M., Nanda, R., et al. (2019). Pembrolizumab monotherapy for previously treated metastatic triple-negative breast cancer: cohort A of the phase II KEYNOTE-086 study. Ann. Oncol. *30*, 397–404. https://doi.org/10.1093/annonc/mdy517.

40. Schmid, P., Adams, S., Rugo, H.S., Schneeweiss, A., Barrios, C.H., Iwata, H., Diéras, V., Hegg, R., Im, S.A., Shaw Wright, G., et al. (2018). Atezolizumab and nab-paclitaxel in advanced triple-negative breast cancer. N. Engl. J. Med. *379*, 2108–2121. https://doi.org/10.1056/NEJMoa1809615.

41. Schmid, P., Cortes, J., Pusztai, L., McArthur, H., Kümmel, S., Bergh, J., Denkert, C., Park, Y.H., Hui, R., Harbeck, N., et al. (2020). Pembrolizumab for early triple-negative breast cancer. N. Engl. J. Med. *382*, 810–821. https://doi.org/10.1056/NEJMoa1910549.

42. Wolchok, J.D., Chiarion-Sileni, V., Gonzalez, R., Rutkowski, P., Grob, J.-J., Cowey, C.L., Lao, C.D., Wagstaff, J., Schadendorf, D., Ferrucci, P.F., et al. (2017). Overall survival with combined nivolumab and ipilimumab in advanced melanoma. N. Engl. J. Med. *377*, 1345–1356. https://doi.org/10.1056/NEJMoa1709684.

43. Loi, S., Schmid, P., Cortés, J., Cescon, D.W., Winer, E.P., Toppmeyer, D., Rugo, H.S., Laurentiis, M.D., Nanda, R., Iwata, H., et al. (2019). Abstract LB-225: RNA molecular signatures as predictive biomarkers of response to monotherapy pembrolizumab in patients with metastatic triple-negative breast cancer: KEYNOTE-086. Cancer Res. *79*, LB-225. https://doi.org/10.1158/1538-7445.Am2019-lb-225.

44. Mackay, L.K., Minnich, M., Kragten, N.A.M., Liao, Y., Nota, B., Seillet, C., Zaid, A., Man, K., Preston, S., Freestone, D., et al. (2016). Hobit and Blimp1 instruct a universal transcriptional program of tissue residency in lymphocytes. Science *352*, 459–463. https://doi.org/10.1126/science.aad2035.

45. Yang, K., and Kallies, A. (2021). Tissue-specific differentiation of CD8(+) resident memory T cells. Trends Immunol. *42*, 876–890. https://doi.org/10.1016/j.it.2021.08.002.

46. Mackay, L.K., Wynne-Jones, E., Freestone, D., Pellicci, D.G., Mielke, L.A., Newman, D.M., Braun, A., Masson, F., Kallies, A., Belz, G.T., and Carbone, F.R. (2015). T-Box transcription factors combine with the cytokines TGF-beta and IL-15 to control tissue-resident memory T cell fate. Immunity *43*, 1101–1111. https://doi.org/10.1016/j.immuni.2015.11.008.

47. Ma, C., Mishra, S., Demel, E.L., Liu, Y., and Zhang, N. (2017). TGF-B controls the formation of kidney-resident T cells via promoting effector T cell extravasation. J. Immunol. *198*, 749–756. https://doi.org/10.4049/jimmunol.1601500.

48. Nizard, M., Roussel, H., Diniz, M.O., Karaki, S., Tran, T., Voron, T., Dransart, E., Sandoval, F., Riquet, M., Rance, B., et al. (2017). Induction of resident memory T cells enhances the efficacy of cancer vaccine. Nat. Commun. *8*, 15221. https://doi.org/10.1038/ncomms15221.

49. Zhang, N., and Bevan, M.J. (2013). Transforming growth factor-β signaling controls the formation and maintenance of gut-resident memory T cells by regulating migration and retention. Immunity *39*, 687–696. https://doi.org/10.1016/j.immuni.2013.08.019.

50. Boutet, M., Gauthier, L., Leclerc, M., Gros, G., de Montpreville, V., Théret, N., Donnadieu, E., and Mami-Chouaib, F. (2016). TGFbeta signaling intersects with CD103 integrin signaling to promote T-lymphocyte accumulation and antitumor activity in the lung tumor microenvironment. Cancer Res. *76*, 1757–1769. https://doi.org/10.1158/0008-5472.can-15-1545.

51. El-Asady, R., Yuan, R., Liu, K., Wang, D., Gress, R.E., Lucas, P.J., Drachenberg, C.B., and Hadley, G.A. (2005). TGF-{beta}-dependent CD103 expression by CD8(+) T cells promotes selective destruction of the host intestinal epithelium during graft-versus-host disease. J. Exp. Med. *201*, 1647–1657. https://doi.org/10.1084/jem.20041044.

52. Laidlaw, B.J., Zhang, N., Marshall, H.D., Staron, M.M., Guan, T., Hu, Y., Cauley, L.S., Craft, J., and Kaech, S.M. (2014). CD4+ T cell help guides formation of CD103+ lung-resident memory CD8+ T cells during influenza viral infection. Immunity *41*, 633–645. https://doi.org/10.1016/j.immuni.2014.09.007.

53. Reis, B.S., Hoytema van Konijnenburg, D.P., Grivennikov, S.I., and Mucida, D. (2014). Transcription factor T-bet regulates intraepithelial lymphocyte functional maturation. Immunity *41*, 244–256. https://doi.org/10.1016/j.immuni.2014.06.017.

54. Adachi, T., Kobayashi, T., Sugihara, E., Yamada, T., Ikuta, K., Pittaluga, S., Saya, H., Amagai, M., and Nagao, K. (2015). Hair follicle-derived IL-7 and IL-15 mediate skin-resident memory T cell homeostasis and lymphoma. Nat. Med. *21*, 1272–1279. https://doi.org/10.1038/nm.3962.

55. Strutt, T.M., Dhume, K., Finn, C.M., Hwang, J.H., Castonguay, C., Swain, S.L., and McKinstry, K.K. (2018). IL-15 supports the generation of protective lung-resident memory CD4 T cells. Mucosal Immunol. *11*, 668–680. https://doi.org/10.1038/mi.2017.101.

56. Schenkel, J.M., Fraser, K.A., Casey, K.A., Beura, L.K., Pauken, K.E., Vezys, V., and Masopust, D. (2016). IL-15-Independent maintenance of tissue-resident and boosted effector memory CD8 T cells. J. Immunol. *196*, 3920–3926. https://doi.org/10.4049/jimmunol.1502337.

57. Bosiljcic, M., Cederberg, R.A., Hamilton, M.J., LePard, N.E., Harbourne, B.T., Collier, J.L., Halvorsen, E.C., Shi, R., Franks, S.E., Kim, A.Y., et al. (2019). Targeting myeloid-derived suppressor cells in combination with

primary mammary tumor resection reduces metastatic growth in the lungs. Breast Cancer Res. *21*, 103. https://doi.org/10.1186/s13058-019-1189-x.

58. Beavis, P.A., Milenkovski, N., Henderson, M.A., John, L.B., Allard, B., Loi, S., Kershaw, M.H., Stagg, J., and Darcy, P.K. (2015). Adenosine receptor 2A blockade increases the efficacy of anti-PD-1 through enhanced anti-tumor T-cell responses. Cancer Immunol. Res. *3*, 506–517. https://doi.org/10.1158/2326-6066.Cir-14-0211.

59. Le Naour, A., Koffi, Y., Diab, M., Le Guennec, D., Rougé, S., Aldekwer, S., Goncalves-Mendes, N., Talvas, J., Farges, M.-C., Caldefie-Chezet, F., et al. (2020). EO771, the first luminal B mammary cancer cell line from C57BL/6 mice. Cancer Cell Int. *20*, 328. https://doi.org/10.1186/s12935-020-01418-1.

60. Gálvez-Cancino, F., López, E., Menares, E., Díaz, X., Flores, C., Cáceres, P., Hidalgo, S., Chovar, O., Alcántara-Hernández, M., Borgna, V., et al. (2018). Vaccination-induced skin-resident memory CD8(+) T cells mediate strong protection against cutaneous melanoma. OncoImmunology *7*, e1442163. https://doi.org/10.1080/2162402x.2018.1442163.

61. Man, K., Gabriel, S.S., Liao, Y., Gloury, R., Preston, S., Henstridge, D.C., Pellegrini, M., Zehn, D., Berberich-Siebelt, F., Febbraio, M.A., et al. (2017). Transcription factor IRF4 promotes CD8(+) T cell exhaustion and limits the development of memory-like T cells during chronic infection. Immunity *47*, 1129–1141.e5. https://doi.org/10.1016/j.immuni.2017.11.021.

62. Miller, B.C., Sen, D.R., Al Abosy, R., Bi, K., Virkud, Y.V., LaFleur, M.W., Yates, K.B., Lako, A., Felt, K., Naik, G.S., et al. (2019). Subsets of exhausted CD8(+) T cells differentially mediate tumor control and respond to checkpoint blockade. Nat. Immunol. *20*, 326–336. https://doi.org/10.1038/s41590-019-0312-6.

63. Beumer-Chuwonpad, A., Taggenbrock, R.L.R.E., Ngo, T.A., and van Gisbergen, K.P.J.M. (2021). The potential of tissue-resident memory T cells for adoptive immunotherapy against cancer. Cells *10*, 2234.

64. Jaiswal, A., Verma, A., Dannenfelser, R., Melssen, M., Tirosh, I., Izar, B., Kim, T.G., Nirschl, C.J., Devi, K.S.P., Olson, W.C., Jr., et al. (2022). An activation to memory differentiation trajectory of tumor-infiltrating lymphocytes informs metastatic melanoma outcomes. Cancer Cell *40*, 524–544.e5. https://doi.org/10.1016/j.ccell.2022.04.005.

65. Curtis, C., Shah, S.P., Chin, S.-F., Turashvili, G., Rueda, O.M., Dunning, M.J., Speed, D., Lynch, A.G., Samarajiwa, S., Yuan, Y., et al. (2012). The genomic and transcriptomic architecture of 2,000 breast tumours reveals novel subgroups. Nature *486*, 346–352. https://doi.org/10.1038/nature10983.

66. Wolf, D.M., Yau, C., Wulfkuhle, J., Brown-Swigart, L., Gallagher, R.I., Lee, P.R.E., Zhu, Z., Magbanua, M.J., Sayaman, R., O'Grady, N., et al. (2022). Redefining breast cancer subtypes to guide treatment prioritization and maximize response: predictive biomarkers across 10 cancer therapies. Cancer Cell *40*, 609–623.e6. https://doi.org/10.1016/j.ccell.2022.05.005.

67. Cortazar, P., Zhang, L., Untch, M., Mehta, K., Costantino, J.P., Wolmark, N., Bonnefoi, H., Cameron, D., Gianni, L., Valagussa, P., et al. (2014). Pathological complete response and long-term clinical benefit in breast cancer: the CTNeoBC pooled analysis. Lancet (London, England) *384*, 164–172. https://doi.org/10.1016/s0140-6736(13)62422-8.

68. Loibl, S., Schneeweiss, A., Huober, J., Braun, M., Rey, J., Blohmer, J.U., Furlanetto, J., Zahm, D.M., Hanusch, C., Thomalla, J., et al. (2022). Neoadjuvant durvalumab improves survival in early triple-negative breast cancer independent of pathological complete response. Ann. Oncol. *33*, 1149–1158. https://doi.org/10.1016/j.annonc.2022.07.1940.

69. Liu, D., Schilling, B., Liu, D., Sucker, A., Livingstone, E., Jerby-Arnon, L., Zimmer, L., Gutzmer, R., Satzger, I., Loquai, C., et al. (2019). Integrative molecular and clinical modeling of clinical outcomes to PD1 blockade in patients with metastatic melanoma. Nat. Med. *25*, 1916–1927. https://doi.org/10.1038/s41591-019-0654-5.

70. Topalian, S.L., Drake, C.G., and Pardoll, D.M. (2015). Immune checkpoint blockade: a common denominator approach to cancer therapy. Cancer Cell *27*, 450–461. https://doi.org/10.1016/j.ccell.2015.03.001.

71. Loi, S., Sirtaine, N., Piette, F., Salgado, R., Viale, G., Van Eenoo, F., Rouas, G., Francis, P., Crown, J.P.A., Hitre, E., et al. (2013). Prognostic and predictive value of tumor-infiltrating lymphocytes in a phase III randomized adjuvant breast cancer trial in node-positive breast cancer comparing the addition of docetaxel to doxorubicin with doxorubicin-based chemotherapy: BIG 02-98. J. Clin. Oncol. *31*, 860–867. https://doi.org/10.1200/jco.2011.41.0902.

72. Schmid, P., Cortes, J., Dent, R., Pusztai, L., McArthur, H., Kümmel, S., Bergh, J., Denkert, C., Park, Y.H., Hui, R., et al. (2022). Event-free survival with pembrolizumab in early triple-negative breast cancer. N. Engl. J. Med. *386*, 556–567. https://doi.org/10.1056/NEJMoa2112651.

73. Cortes, J., Rugo, H.S., Cescon, D.W., Im, S.A., Yusof, M.M., Gallardo, C., Lipatov, O., Barrios, C.H., Perez-Garcia, J., Iwata, H., et al. (2022). Pembrolizumab plus chemotherapy in advanced triple-negative breast cancer. N. Engl. J. Med. *387*, 217–226. https://doi.org/10.1056/NEJMoa2202809.

74. Webb, J.R., Milne, K., and Nelson, B.H. (2015). PD-1 and CD103 are widely coexpressed on prognostically favorable intraepithelial CD8 T cells in human Ovarian cancer. Cancer Immunol. Res. *3*, 926–935. https://doi.org/10.1158/2326-6066.CIR-14-0239.

75. Christo, S.N., Evrard, M., Park, S.L., Gandolfo, L.C., Burn, T.N., Fonseca, R., Newman, D.M., Alexandre, Y.O., Collins, N., Zamudio, N.M., et al. (2021). Discrete tissue microenvironments instruct diversity in resident memory T cell function and plasticity. Nat. Immunol. *22*, 1140–1151. https://doi.org/10.1038/s41590-021-01004-1.

76. Seo, W., Jerin, C., and Nishikawa, H. (2021). Transcriptional regulatory network for the establishment of CD8+ T cell exhaustion. Exp. Mol. Med. *53*, 202–209. https://doi.org/10.1038/s12276-021-00568-0.

77. Adams, S., Loi, S., Toppmeyer, D., Cescon, D.W., De Laurentiis, M., Nanda, R., Winer, E.P., Mukai, H., Tamura, K., Armstrong, A., et al. (2019). Pembrolizumab monotherapy for previously untreated, PD-L1-positive, metastatic triple-negative breast cancer: cohort B of the phase II KEYNOTE-086 study. Ann. Oncol. *30*, 405–411. https://doi.org/10.1093/annonc/mdy518.

78. Luoma, A.M., Suo, S., Wang, Y., Gunasti, L., Porter, C.B.M., Nabilsi, N., Tadros, J., Ferretti, A.P., Liao, S., Gurer, C., et al. (2022). Tissue-resident memory and circulating T cells are early responders to pre-surgical cancer immunotherapy. Cell *185*, 2918–2935.e29. https://doi.org/10.1016/j.cell.2022.06.018.

79. Zehn, D., Thimme, R., Lugli, E., de Almeida, G.P., and Oxenius, A. (2022). 'Stem-like' precursors are the fount to sustain persistent CD8+ T cell responses. Nat. Immunol. *23*, 836–847. https://doi.org/10.1038/s41590-022-01219-w.

80. Pusztai, L., Denkert, C., O'Shaughnessy, J., Cortes, J., Dent, R.A., McArthur, H.L., Kuemmel, S., Bergh, J.C.S., Park, Y.H., Hui, R., et al. (2022). Event-free survival by residual cancer burden after neoadjuvant pembrolizumab + chemotherapy versus placebo + chemotherapy for early TNBC: exploratory analysis from KEYNOTE-522. J. Clin. Oncol. *40*, 503. https://doi.org/10.1200/JCO.2022.40.16_suppl.503.

81. Ritchie, M.E., Phipson, B., Wu, D., Hu, Y., Law, C.W., Shi, W., and Smyth, G.K. (2015). Limma powers differential expression analyses for RNA-sequencing and microarray studies. Nucleic Acids Res. *43*, e47. https://doi.org/10.1093/nar/gkv007.

82. Gao, J., Aksoy, B.A., Dogrusoz, U., Dresdner, G., Gross, B., Sumer, S.O., Sun, Y., Jacobsen, A., Sinha, R., Larsson, E., et al. (2013). Integrative analysis of complex cancer genomics and clinical profiles using the cBioPortal. Sci. Signal. *6*, pl1. https://doi.org/10.1126/scisignal.2004088.

83. Gendoo, D.M.A., Ratanasirigulchai, N., Schröder, M.S., Paré, L., Parker, J.S., Prat, A., and Haibe-Kains, B. (2016). Genefu: an R/Bioconductor package for computation of gene expression-based signatures in breast cancer. Bioinformatics *32*, 1097–1099. https://doi.org/10.1093/bioinformatics/btv693.

84. Robin, X., Turck, N., Hainard, A., Tiberti, N., Lisacek, F., Sanchez, J.-C., and Müller, M. (2011). pROC: an open-source package for R and S+ to

analyze and compare ROC curves. BMC Bioinf. *12*, 77. https://doi.org/10.1186/1471-2105-12-77.

85. Bray, N.L., Pimentel, H., Melsted, P., and Pachter, L. (2016). Near-optimal probabilistic RNA-seq quantification. Nat. Biotechnol. *34*, 525–527. https://doi.org/10.1038/nbt.3519.
86. Soneson, C., Love, M.I., and Robinson, M.D. (2015). Differential analyses for RNA-seq: transcript-level estimates improve gene-level inferences. F1000Res. *4*, 1521. https://doi.org/10.12688/f11000research.17563.12681.
87. Law, C.W., Chen, Y., Shi, W., and Smyth, G.K. (2014). voom: precision weights unlock linear model analysis tools for RNA-seq read counts. Genome Biol. *15*, R29. https://doi.org/10.1186/gb-2014-15-2-r29.
88. Beavis, P.A., Henderson, M.A., Giuffrida, L., Davenport, A.J., Petley, E.V., House, I.G., Lai, J., Sek, K., Milenkovski, N., John, L.B., et al. (2018). Dual PD-1 and CTLA-4 checkpoint blockade promotes antitumor immune responses through CD4+Foxp3− cell–mediated modulation of CD103+ dendritic cells. Cancer Immunol. Res. *6*, 1069–1081. https://doi.org/10.1158/2326-6066.Cir-18-0291.
89. Lai, J., Mardiana, S., House, I.G., Sek, K., Henderson, M.A., Giuffrida, L., Chen, A.X.Y., Todd, K.L., Petley, E.V., Chan, J.D., et al. (2020). Adoptive cellular therapy with T cells expressing the dendritic cell growth factor Flt3L drives epitope spreading and antitumor immunity. Nat. Immunol. *21*, 914–926. https://doi.org/10.1038/s41590-020-0676-7.
90. Loibl, S., Untch, M., Burchardi, N., Huober, J., Sinn, B.V., Blohmer, J.U., Grischke, E.M., Furlanetto, J., Tesch, H., Hanusch, C., et al. (2019). A randomised phase II study investigating durvalumab in addition to an anthracycline taxane-based neoadjuvant therapy in early triple-negative breast cancer: clinical results and biomarker analysis of GeparNuevo study. Ann. Oncol. *30*, 1279–1288. https://doi.org/10.1093/annonc/mdz158.
91. Kim, D., Paggi, J.M., Park, C., Bennett, C., and Salzberg, S.L. (2019). Graph-based genome alignment and genotyping with HISAT2 and HISAT-genotype. Nat. Biotechnol. *37*, 907–915. https://doi.org/10.1038/s41587-019-0201-4.
92. Anders, S., Pyl, P.T., and Huber, W. (2015). HTSeq—a Python framework to work with high-throughput sequencing data. Bioinformatics *31*, 166–169. https://doi.org/10.1093/bioinformatics/btu638.
93. Molania, R., Gagnon-Bartsch, J.A., Dobrovic, A., and Speed, T.P. (2019). A new normalization for Nanostring nCounter gene expression data. Nucleic Acids Res. *47*, 6073–6083. https://doi.org/10.1093/nar/gkz433.
94. McCarthy, D.J., Chen, Y., and Smyth, G.K. (2012). Differential expression analysis of multifactor RNA-Seq experiments with respect to biological variation. Nucleic Acids Res. *40*, 4288–4297. https://doi.org/10.1093/nar/gks042.
95. Wickham, H. (2016). ggplot2: Elegant Graphics for Data Analysis (Springer-Verlag New York).
96. Gu, Z., Eils, R., and Schlesner, M. (2016). Complex heatmaps reveal patterns and correlations in multidimensional genomic data. Bioinformatics *32*, 2847–2849. https://doi.org/10.1093/bioinformatics/btw313.
97. Stoeckius, M., Zheng, S., Houck-Loomis, B., Hao, S., Yeung, B.Z., Mauck, W.M., 3rd, Smibert, P., and Satija, R. (2018). Cell Hashing with barcoded antibodies enables multiplexing and doublet detection for single cell genomics. Genome Biol. *19*, 224. https://doi.org/10.1186/s13059-018-1603-1.
98. Hafemeister, C., and Satija, R. (2019). Normalization and variance stabilization of single-cell RNA-seq data using regularized negative binomial regression. Genome Biol. *20*, 296. https://doi.org/10.1186/s13059-019-1874-1.
99. Aibar, S., González-Blas, C.B., Moerman, T., Huynh-Thu, V.A., Imrichova, H., Hulselmans, G., Rambow, F., Marine, J.C., Geurts, P., Aerts, J., et al. (2017). SCENIC: single-cell regulatory network inference and clustering. Nat. Methods *14*, 1083–1086. https://doi.org/10.1038/nmeth.4463.
100. Blake, J.A., Baldarelli, R., Kadin, J.A., Richardson, J.E., Smith, C.L., and Bult, C.J.; Mouse Genome Database Group (2021). Mouse genome Database (MGD): knowledgebase for mouse-human comparative biology. Nucleic Acids Res. *49*, D981–D987. https://doi.org/10.1093/nar/gkaa1083.
101. Korotkevich, G., Sukhov, V., Budin, N., Shpak, B., Artyomov, M., and Sergushichev, A. (2016). Fast gene set enrichment analysis. Preprint at bioRxiv. https://doi.org/10.1101/060012.
102. Laboratory, N.-R.A. (2015). Weather Forecast Verification Utilities. 2015-07-15 01:30:51.
103. Karn, T., Denkert, C., Weber, K.E., Holtrich, U., Hanusch, C., Sinn, B.V., Higgs, B.W., Jank, P., Sinn, H.P., Huober, J., et al. (2020). Tumor mutational burden and immune infiltration as independent predictors of response to neoadjuvant immune checkpoint inhibition in early TNBC in GeparNuevo. Ann. Oncol. *31*, 1216–1222. https://doi.org/10.1016/j.annonc.2020.05.015.
104. Jiang, H., Lei, R., Ding, S.-W., and Zhu, S. (2014). Skewer: a fast and accurate adapter trimmer for next-generation sequencing paired-end reads. BMC Bioinf. *15*, 182. https://doi.org/10.1186/1471-2105-15-182.
105. Therneau, T. (2021). A Package for Survival Analysis in R. R Package Version 3.2-13.

STAR★METHODS

KEY RESOURCES TABLE

REAGENT or RESOURCE	SOURCE	IDENTIFIER
Antibodies		
Brilliant Violet 711anti-mouse CD8a antibody (Clone: 53-6.7)	BioLegend	Cat# 10074; RRID: AB_11219594
PE/Cyanine7 anti-mouse CD8a antibody (Clone: 53-6.7)	BD Biosciences	Cat# 25-0081-82; RRID: AB_469584
BUV737 anti-Mouse CD8a antibody (Clone: 53-6.7)	BD Biosciences	Cat# 564297; RRID: AB_2722580
BUV737 anti-mouse CD4 antibody (Clone: GK1.5)	eBioscience	Cat# 25-0041-82; RRID: AB_469576
BV421 anti-mouse CD103 antibody (Clone: 2.E7)	eBioscience	Cat# 121422; RRID: AB_2562901
PE anti-mouse CD103 antibody (Clone: 2.E7)	BioLegend	Cat#; 12-1031-83; RRID: AB_465800
FITC anti-mouse CD103 antibody (Clone: 2.E7)	BioLegend	Cat# 562974; RRID: AB_10714791
PerCP/Cyanine5.5 anti-mouse CD103 antibody (Clone: 2.E7)	BioLegend	Cat# 121416; RRID: AB_2128621
PE/Cyanine7 anti-mouse CD45.1 antibody (Clone: A20)	BioLegend	Cat# 110715; RRID: AB_1134168
APC/Cyanine7 anti-mouse CD45.2 antibody (Clone: 104.2)	eBioscience	Cat#109824; RRID: AB_830788
APC anti-mouse CD45.2 antibody (Clone: 104.2)	Milteny Biotec	Cat# 130-102-964; RRID: AB_2660720
Pacific Blue anti-mouse TCR-Vα2 antibody (Clone: 17A2)	eBioscience	Cat# 562944; RRID: AB_2737910
PerCP/Cyanine5.5 anti-mouse TCR-β antibody (Clone: H57.597)	eBioscience	Cat# 45-5961-82; RRID: AB_925763
APC anti-mouse TCR-β antibody (Clone: H57.597)	eBioscience	Cat# 17-5961-83; RRID: AB_469482
PE/Cyanine7 anti-mouse TCR-β antibody (Clone: H57.597)	eBioscience	Cat# 506324; RRID: AB_2256076
BB700 anti-mouse TCR-β antibody (Clone: H57.597)	BD Biosciences	Cat# 745846; RRID: AB_2743291
Alexa Fluor 700 anti-mouse CD3 antibody (Clone: 17A2)	R and D Systems	Cat# FAB4841N; RRID: AB_10994181
PE/Cyanine7 anti-mouse CD62L antibody (Clone: MEL.14)	eBioscience	Cat# 104418; RRID: AB_313103
BV510 anti-mouse CD62L antibody (Clone: MEL.14)	BD Biosciences	Cat# 563117; RRID: AB_2738013
BUV395 anti-mouse CD69 antibody (Clone: H1.2F3)	BD Biosciences	Cat# 740220; RRID: AB_2739968
PE anti-mouse CD69 antibody (Clone: H1.2F3)	eBioscience	Cat# 12-0691-82; RRID: AB_465732
Biotin anti-mouse CD69 antibody (Clone: H1.2F3)	eBioscience	Cat# 104504; RRID: AB_313107
PECF594 anti-mouse CD69 antibody (Clone: H1.2F3)	BD Biosciences	Cat# 562455; RRID: AB_11154217
BV605 anti-mouse CD44 antibody (Clone: 516.10A1)	BioLegend	Cat# 103047; RRID: AB_2562451

(*Continued on next page*)

Continued

REAGENT or RESOURCE	SOURCE	IDENTIFIER
BV395 anti-mouse CD44 antibody (Clone: IM7)	BD Biosciences	Cat# 740215; RRID: AB_2739963
BV711 anti-mouse PD-1 antibody (CD279) (Clone: J43)	BD Biosciences	Cat# 744547; RRID: AB_2742318
FITC anti-mouse PD-1 antibody (CD279) (Clone: J43)	eBiocience	Cat# 11-9985-85; RRID: AB_465473
eFluor 450 anti-mouse PD-1 antibody (CD279) (Clone: FJK.16s)	eBiocience	Cat# 48-5773-82; RRID: AB_1518812
APC anti-mouse IFN-γ antibody (Clone: XMG1.2)	eBiocience	Cat# 17-7311-82; RRID: AB_469504
BV605 anti-mouse IFN-γ antibody (Clone: XMG1.2)	eBiocience	Cat# 505839; RRID: AB_2561438
BV785 anti-mouse TNF-α antibody (Clone: MP6.XT22)	BioLegend	Cat# 506341; RRID: AB_2565951
AF488 anti-mouse Eomes antibody (Clone: DAN11MAG)	eBiocience	Cat# 53-4875-80; RRID: AB_10853025
PE anti-mouse Tox antibody (Clone: REA473)	Milteny Biotec	Cat# 130-120-716; RRID: AB_2801780
APC SIINFEKL antibody (Clone: 25-D1.16)	BioLegend	Cat# 141606; RRID: AB_11219595
PE/Cyanine7 Streptavidin	eBioscience	Cat# 25-4317-82; RRID: AB_10116480
BV785 Streptavidin	BD Biosciences	Cat# 5405249; RRID: AB_2869529
InVivo MAb anti-Mouse PD-1 (CD279) antibody (Clone: RMP1.14)	BioXCell	Cat# BE0146; RRID: AB_10949053
InVivo MAb anti-Mouse CTLA-4 (CD152) antibody (Clone: 9H10)	BioXCell	Cat# BE0131; RRID: AB_10950184
InVivo MAb rat anti-Mouse IgG2a antibody (Clone: 2A3)	BioXCell	Cat# BE0089; RRID: AB_1107769
Anti-Mouse TNF-α antibody (Clone: MP6.XT22)	BioLegend	Cat# 510802; RRID: AB_315567
Purified anti-Mouse IFN-γ antibody (Clone: XMG1.2)	BioLegend	Cat# 505802; RRID: AB_315396
Purified Rat IgG1, κ Isotype antibody (Clone: R3-34)	BD Biosciences	Cat# 397192; RRID: AB_397192
Anti-Mouse IFN-γ antibody (Clone: R3-34)	BD Biosciences	Cat# 554412; RRID: AB_395376
Anti-Mouse TNF-α antibody (Clone: MP6.XT22)	BD Biosciences	Cat# 554419; RRID: AB_395380
Mouse Fc Block purified antibody (Clone:2.4G2)	BD Biosciences	Cat# 553142; RRID: AB_394656
Chemicals, peptides, and recombinant proteins		
Deoxyribonuclease I (DNase I)	Roche Scientific	Cat# 4716728001; RRID: N/A
Chromium-51 Radionuclide	Perkin Elmer	Cat# 01-2222-41; RRID: N/A
Ovalbumin peptide (OVA 257-264)	GenScript	Cat# RP10611; RRID: N/A
Paraformaldehyde16% w/v aqueous solution	Thermo Fisher Scientific	Cat# 043368.9M; RRID: N/A
FTY-720 Compound	Sapphire Biosciences	Cat# TRC-F810390; RRID: N/A
2-Hydroxypropyl-beta-cyclodextrin	Sapphire Biosciences	Cat# 16169; RRID: N/A
Dulbecco′s Modified Eagle′s Medium (DMEM)	Thermo Fisher Scientific	Cat# 12491015; RRID: N/A
Phorbol 12-Myristate 13-Acetate (PMA)	Sigma Aldrich	Cat# P8139-1MG; RRID: N/A
Ionomycin Salt	Sigma Aldrich	Cat# 2006643; RRID: N/A

(*Continued on next page*)

Continued

REAGENT or RESOURCE	SOURCE	IDENTIFIER
GolgiPlug (Brefeldin A)	BD Biosciences	Cat# 555029; RRID: N/A
GolgiStop (Monensin)	BD Biosciences	Cat# 554724; RRID: N/A
Foxp3/Transcription factor staining buffer set	Invitrogen	Cat# 00-5523-00; RRID: N/A
Fetal Calf serum (FCS)	Thermo Fisher Scientific	Cat# A38401; RRID: N/A
100X penicillin/streptomycin	Thermo Fisher Scientific	Cat# 10378016; RRID: N/A
GlutaMAX Suppliment	Thermo Fisher Scientific	Cat# 35050079; RRID: N/A
Red cell lysis buffer	eBioscience	Cat# 00-4333-57; RRID: N/A
Viability dye-Fix Red	Life Technologies	Cat# 423110; RRID: N/A
Viability dye-Fix Yellow	Life Technologies	Cat# 423104; RRID: N/A
Viability dye- Ghost Red	Cell Signaling	Cat# 18452; RRID: N/A
Critical commercial assays		
Anti-mouse TCR-Vβ Screening Panel	BD Biosciences	Cat# 557004; RRID: AB_647180
Cytometric Bead Array Flex Set	BD Biosciences	Cat# 558340; RRID: AB_2869165
QuantSeq 3' mRNA-Seq Library Prep Kit	Lexogen	Cat# 193-196
NextSeq500 WGS System	Illumina	Cat# SY-415-1001
Chromium Next GEM Single Cell 5' Kit v2	10x Genomics	Cat# CG000331
Deposited data		
Bulk RNA-seq raw files	This paper	NIH BioProject: PRJNA889326
Bulk RNA-seq processed files	This paper	GEO: GSE218161
scRNA-seq raw files	This Paper	GitHub data: https://github.com/LoiLab
scRNA-seq processed files	This Paper	GitHub data: https://github.com/LoiLab
Human TNBC $CD8^+$ T_{RM} gene signature	Savas et al,[13]	GEO: GSE110686
Murine infection tissue-residency signature	Mackay et al,[44]	GEO: GSE70813
LCMV Core $CD8^+$ T cell exhaustion signature	Man et al,[61]	GEO: GSE84820
LCMV exhausted $CD8^+$ T cell signatures	Miller et al,[62]	GEO: GSE123235
Human Melanoma $CD8^+$ T cell exhaustion signature	Jaiswal et al,[64]	GEO: GSE72056
Clinical data post anti-CTLA-4 and anti-PD-1 therapy	Liu et al,[69]	DbGaP: phs000452.v3.p1
Clinical data post anti-CTLA-4 and anti-PD-1 therapy	Gide et al,[34]	NIH BioProject: PRJEB23709
Experimental models: Cell lines		
Murine TNBC: AT3-OVA and AT3 parental cells	Laboratory of Phil Darcy	N/A
Murine TNBC: AT3 parental cells	Laboratory of Phil Darcy	N/A
Murine TNBC: EO771-OVA cells	Laboratory of Phil Darcy	N/A
Murine TNBC: EO771 parental cells	Laboratory of Phil Darcy	N/A
Murine TNBC: 4T1.2 cells	Laboratory of Phil Darcy	N/A
Experimental models: Organisms/strains		
Mouse: C57BL/6J CD45.2 wild type	The Walter and Eliza Hall Institute of Medical Research	N/A
Mouse: BALB/C wild type	The Walter and Eliza Hall Institute of Medical Research	N/A
Mouse: OTI CD45.1 wild type	The Walter and Eliza Hall Institute of Medical Research	N/A
Mouse: $IL15^{-/-}$ knockout (KO)	The Walter and Eliza Hall Institute of Medical Research	N/A
Mouse: OT-I.CD45.1.TGF-β receptor(R)$II^{-/-}$	The Walter and Eliza Hall Institute of Medical Research	N/A

(*Continued on next page*)

Continued

REAGENT or RESOURCE	SOURCE	IDENTIFIER
Mouse: OT-I.CD45.1.*Tbx21*$^{-/-}$	The Walter and Eliza Hall Institute of Medical Research	N/A
Mouse: OT-I.CD45.1.*Eomes*$^{-/-}$	the Walter and Eliza Hall Institute of Medical Research	N/A
Oligonucleotides		
anti-mouse Hashtag 1 barcode sequence: ACCCACCAGTAAGAC	Biolegend	Cat# C0301
anti-mouse Hashtag 2 barcode sequence: GGTCGAGAGCATTCA	Biolegend	Cat# C0302
anti-mouse Hashtag 4 barcode sequence: AAAGCATTCTTCACG	Biolegend	Cat# C0304
Software and algorithms		
R code associated with scRNA-seq	This paper	GitHub data: https://github.com/LoiLab
GraphPad Prism, version 8	GraphPad Software. Inc.	https://www.graphpad.com/
FlowJo Software v10.8.1	BD Biosciences	Cat# 23-21733-01
FCAP Array Software v3.0	BD Biosciences	Cat# 23-15075-03
limma Software	Ritchie et al[81]	https://bioinf.wehi.edu.au/limma/
CBioPortal (open source) Software	Gao et al,[82]	https://www.cbioportal.org/
R package genefu Software (version 2.28.0)	Gendoo et al,[83]	https://www.r-project.org/
R package pROC Software	Robin et al,[84]	https://www.r-project.org/
kallisto Software (version 0.46.0)	Bray et al,[85]	https://bioweb.pasteur.fr/packages/pack@kallisto@0.46.0
Tximport Software	Soneson et al,[86]	https://github.com/mikelove/tximport
limma voom Software	Law et al,[87]	https://github.com/ben-laufer/RNA-seq/blob/main/04-limma-voom.R
Other		
Liquid-Counting Beads	BD Biosciences	Cat# 335925; RRID: N/A
Ultra-Compensation Beads	Thermo Fisher Scientific	Cat# 01-2222-41; RRID: N/A

RESOURCE AVAILABILITY

Lead contact

Further information and requests for resources and reagents should be directed to and will be fulfilled by the lead contact, Professor Sherene Loi (sherene.loi@petermac.org).

Materials availability

This study did not generate new unique reagents.

Data and code availability

This paper analyzes existing, publicly available data from the original research article and accession numbers for the external datasets are indicated in the key resources table as well as in the Gene set enrichment methods (GSEA), refer to STAR Methods.

Bulk RNA-seq data both unprocessed and processed reads related to Figure 1 have been deposited at Database: NIH BioProject: PRJNA889326 (http://www.ncbi.nlm.nih.gov/bioproject/889326) and GEO: GSE218161 (https://www.ncbi.nlm.nih.gov/geo/query/acc.cgi?acc=GSE218161) respectively, and are publicly available as of the date of publication. The R source code, processed and raw data for scRNA-seq analyses related to Figure 2 as well as the survival analyses presented in Figure 5 are available in GitHub data: https://github.com/LoiLab and indicated in the key resources table. The authors declare, all new deposited data, R source codes will be made accessible to readers upon publication and all other data that support the findings of this study are available with the manuscript supplemental information, and any additional information- is available from the lead contact upon request.

EXPERIMENTAL MODEL AND SUBJECT DETAILS

Mouse cell lines

The murine TNBC cell lines AT3-OVA, AT3 parental, 4T1.2, EO771-OVA and EO771 parental cells were provided by Prof. Phil Darcy (Peter MacCallum Cancer Centre, Melbourne, VIC, Australia). AT3-OVA and EO771-OVA TNBC cells were generated by transducing the parental AT3 and EO771 cells with a retroviral vector, pMIG/MSCV-IRES-eGFP plasmid encoding membrane-bound chicken ovalbumin (OVA) protein, tagged with GFP in the laboratory of Prof. Phil Darcy and cultured as previously described.[88,89] All cell lines were cultured with complete DMEM media supplemented with 10% FCS, 1% Penicillin, 1% GlutaMAX Supplement. Cells were grown at 37°C with 5% CO2 in a humidified sterile incubator. For all *in vivo* experiments, $5x10^5$ of AT3-OVA cells or $2.5x10^5$ of 4T1.2, AT3 parental, EO771-OVA and EO771 parental cells at early passages were resuspended in 50 μL phosphate buffer saline (PBS) solution at neutral pH for mammary fat pad (MFP) injections. All cell lines were tested regularly and verified to be mycoplasma negative at the Victorian Infectious Diseases References Lab (Melbourne, VIC, Australia).

Mouse models

All animal experiments conducted in this study were approved by the relevant Peter MacCallum Cancer Centre Animal Experimentation Ethics Committee or by The University of Melbourne Animal Ethics Committee and conducted in accordance with the National Health and Medical Research Council Australian Code of Practice for the Care and Use of Animals for Scientific Purposes. We used seven-to eight-weeks old female C57BL/6J mice AT3-OVA, EO771 cells and female BALB/C mice for 4T1.2 TNBC experiments. TNBC cells were injected orthotopically in the 4^{th} mammary fat pad of respective mice background and tumor volume (length x width2 x 0.5) was calculated by vernier caliper following development of palpable tumors and measurements were taken every 3-4 days. The tumor measurements were reported as mm^3, mean ± SEM of individual tumor volume. At the experimental end points (Figure 3), mice were euthanized when the tumors reached an ethical limit of 1500 mm^3 or if the animals showed signs of any adverse health indications that met the Peter MacCallum cancer center institutional criteria for sacrifice. For *in vivo* mechanistic experiments reported in Figure 1, C57BL/6J wild type (WT), $IL15^{-/-}$ knockout (KO) mice and the OTI WT, OT-I.CD45.1.TGF-β receptor(R)II$^{-/-}$ or OT-I.CD45.1.*Tbx21*$^{-/-}$or OT-I.CD45.1.*Eomes*$^{-/-}$ transgenic mice strains were used and obtained from the Walter and Eliza Hall Institute of Medical Research and the Department of Microbiology and Immunology of The University of Melbourne (VIC, Australia). The criteria of mice from the analyses, when applied, have been indicated in the figure legends. The investigators did not perform any experiments in blind, and the animals were not previously involved in other experimental procedures.

Human studies

The study participants in GeparNuevo (NCT02685059) described in Figure 5, a multicentre, prospective, randomised, double-blind, placebo-controlled phase II trial examining the efficacy of nab-paclitaxel, followed by dose-dense epirubicin/cyclophosphamide with durvalumab versus placebo in patients with non-metastatic primary TNBC. This study was approved by the ethics committee and authority and the study criteria including the protocol for approval and informed consent have been previously published.[68,90] The RNA-seq data was available for 162 patients out of a sample size of 174 enrolled in the trial and were used in clinical cohort analyses.

METHOD DETAILS

Adoptive transfer of transgenic CD8$^+$ T cells

Naive OT-I cells were isolated from lymph nodes of OTI WT, OT-I.CD45.1.TGF-β receptor(R)II$^{-/-}$ or OT-I.CD45.1.*Tbx21*$^{-/-}$or OT-I.CD45.1.*Eomes*$^{-/-}$ transgenic donor mice and intravenously transferred to recipient C57BL/6J mice. For experiments reported in Figure 1, a total of 2.5×10^5 cells per population were transferred in co-transfer experiments. *In vitro*–generated effector OT-I cells were activated by ovalbumin peptide ($OVA_{257-264}$) (1mg/ml; GenScript, New Jersey, USA) and cultured for 4 days. On days 2 and 3, cultures were split 1:2 and IL-2 (10 U/ml) was added. For experiments with $IL15^{-/-}$ knockout (KO) mice, 5×10^5 day 4 i*n vitro*–generated effector OT-I cells were transferred intravenously to recipient mice as indicated. At the end of the experiments, tumors in the mammary fat pad (MFP) excluding tumor draining lymph nodes and spleen of mice were collected for *ex vivo* FACS analysis of tumor-infiltrating lymphocytes (TILs) and resident CD8$^+$ T cell sub-populations. The sample size and statistical tests of computation are indicated in respective figure legend.

Treatment of tumor bearing mice

For experiments reported in Figures 3 and 4, C57BL/6J mice were orthotopically injected with $5x10^5$ AT3-OVA TNBC cells in the 4^{th} MFP. When tumors were palpable with an average tumor volume of 25-50 mm^3, 10-11 days after TNBC cell inoculation, mice were randomized and treated with vehicle (anti-2A3, 200 ug/dose), anti-PD-1 (200ug/dose) or/and anti-CTLA-4 (150ug /dose) in combination were administered intraperitoneally at three days interval and the tumor growth efficacy and survival of mice were monitored until the experimental endpoint. A total of two doses of indicated ICB antibodies were administered prior to tumor excision on d28 for FACS analysis of TILs, TCR-Vβ epitope analyses, and FACS sorting of resident memory CD8$^+$ T cell sub-populations for chromium assays. Experiments examining the tissue-protective effects of tissue- resident memory CD8$^+$ T cells (Figure 4), tumor-free mice post four doses of ICB treatment were rechallenged with AT3-OVA cells on d40 post primary BC inoculation. Two days prior to tumor re-challenge, mice were administered with FTY-720 (Sapphire Biosciences) in 2% 2-hydroxypropyl-beta-cyclodextrin solution

reconstituted in PBS at a final concentration of 1mg/kg. FTY treatment was initiated two days before BC rechallenge and administered intraperitoneally based on mouse weight and dosed once daily for five days with one-day interval until the experimental endpoint. All experiments were independently repeated at least twice and the total number of mice that completely regressed (undetectable) tumors compared to palpable tumors at endpoint was recorded and tumor weights were determined, and tissues explanted for analysis at the end of the experiments.

FACS analysis of TILs

For FACS experiment in Figures 2 and 3, Mammary tumors were excised on day 28 post BC tumor inoculation without tumor-draining lymph node and were enzymatically digested with 1mg/ml collagenase type IV (Sigma-Aldrich) and 0.02mg/ml DNase (Sigma-Aldrich). After digestion at 37°C for 30 minutes, cells were serially passed through 70-mm and 40-mm filters and followed by FcR blockade (2.4G2) at 1:200 dilution for 10 minutes at 4°C. Spleens of mice were red cell lysed with the use of AKC lysis buffer and filtered through a 70-mm filter prior to FACS staining with surface FACS antibodies and for the use of single-color controls. Tumor samples were stained for TILs and T_{RM} analysis as indicated with respective lineage antibodies (see key resources table). Post staining with antibody cocktail for 45 minutes at 4°C, samples were washed twice with FACS wash buffer (2% FCS in PBS) and fixed with 2% paraformaldehyde. Counting beads (BD Biosciences, USA) (20ul) were added to the homogenized cells in suspension which were then analyzed by flow cytometry (BD Symphony FACS analyzer) for tumor-infiltrating T cells distinguished by $TCR\beta^+$, $CD45^+$ cells and analyzed for $CD44^{hi}CD8^+CD69^+CD103^-$ and $CD44^{hi}CD8^+CD69^+$ $CD103^+$ T_{RM}-like cells, $CD4^+$ $Foxp3^+$ T regulatory cells and H-2Kb-$OVA_{(257-264)}$ SIINFEKL MHC Tetramers were used to study the OVA-reactive $CD8^+$ T cells. For the *in vivo* mechanistic experiment (Figure 1), TCR-Vα2 and congenic markers CD45.1/CD45.2 were used to distinguish WT and transgenic donor $CD8^+$ T cells in tumor-bearing recipient mice. For the analyses of TCR-Vβ repertoire (Figure 3), mammary tumors were isolated following treatments with respective ICB blockade therapy on Day 28 post tumor inoculation (Day 18 post ICB treatments). Tumor samples were processed for single cell suspension as described above and were washed twice prior to *in vitro* staining with the TCR-Vβ FITC-conjugated antibody (BD Biosciences) Fixable Yellow, fixable blue or fixable red (BioLegend, USA) were used as viability dyes for identification of live cells and antibody-stained cell suspension were washed twice and subsequently analyzed by flow cytometry.

Intracellular cytokine staining

TIL samples were stimulated *in vitro* with Phorbol 12-Myristate 13-Acetate (PMA) (50 ng/ml) and Ionomycin (1 μg/ml; Sigma-Aldrich) in the presence of GolgiPlug (BD Biosciences; 1:1000) and GolgiStop (BD Biosciences; 1:1500) for 3-4 hours for experiments reported in Figures 3 and 4. Cells were washed twice and resuspended in FACS wash buffer for staining with cell surface monoclonal antibodies (mAbs), refer to key resources table, and fix permeabilized with Foxp3/Transcription factor staining buffer set (eBioscience, USA) as per the manufacturer's protocol prior to staining with intracellular FOXP3, IFN γ and TNF-α monoclonal antibody (mAb) cocktail for flow cytometry analysis.

Chromium release assay

For *in vitro* cytotoxicity assays (Figure 3) with sodium chromate (^{51}Cr), $2x10^6$ AT3-OVA tumor cells (target) per condition were reconstituted in 200 μL of TIL media (DMEM with 10% FCS, 5% Glutamax, and 5% penicillin/streptomycin) and incubated in the presence of 100 μCi of ^{51}Cr for 1 hour at room temperature. After labeling, cells were washed twice with TIL reconstitution media and plated in sterile 96-well v bottom plates with 100 μL sample per well. The chromium labeled AT3-OVA (target) tumor cells were co-cultured with FACS purified $CD69^+CD103^-$ and $CD69^+CD103^+$ $CD8^+$ T_{RM}-like sub-populations or day4 activated effector OT-I cells as indicated at 5:1 effector/target ratio and cultured for 4 hours and 24 hours separately and in the presence of (10 ng/ml) anti-Isotype, anti-IFN-γ, or anti-TNF-α neutralizing antibodies. Following incubation, the plates were centrifuged, and the cell culture supernatants were collected and the released ^{51}Cr radioactivity was assessed using a 1470 Wizard Automatic Gamma Counter (Wallac, Turku, Finland). Percentage specific lysis of target cells was measured with the proportionate release of ^{51}Cr and was calculated based on $[(^{51}Cr_{assay} - {}^{51}Cr_{spontaneous})/(^{51}Cr_{total} - {}^{51}Cr_{spontaneous}) \times 100]$; $^{51}Cr_{total}$ was measured by direct chromium discharge following complete lysis of BC tumor cells with 1% Triton X-100, and $^{51}Cr_{spontaneous}$ was measured by the release of radioactivity by the tumor cells incubated in the native TIL media in the absence of effector $CD8^+$ T cells.

Cytometric bead array

Cytometric bead array (CBA) experiments in Figure 3, assay was performed on the cell supernatants from the duplicated co-culture wells that were obtained from isotype and dual-ICB treated mouse cohorts as described earlier, and the *in vitro* assay was performed with the use of BD capture beads for IFN-γ and TNF-α according to the BD CBA manufacturer's protocol, refer to key resources table. The samples were incubated for 1 hour at room temperature prior to incubation with detection beads that were conjugated with PE molecule and the samples acquired on BD FACS Verse Systems. Samples and assay standards were analyzed using FCAP array v3 software.

Gene expression analysis

For experiments described in Figures 1 and 2, tumor infiltrating $CD8^+$ T cell sub-populations and splenic-derived naive, effector memory and central memory $CD8^+$ T cell sub-populations ($0.5\text{-}1x10^5$ cells) were FACS purified. Total RNA was extracted from indicated

T cell populations from n=10-15 pooled BC tumors using the RNeasy mini kit (Qiagen) as per the manufacturer's instructions. RNA Tape Station (Agilent, USA) analysis was performed as per the manufacturer's instructions to assess the quantity and quality of RNA present in the sample. 10ng total RNA was used for library preparation according to the manufacturer's instructions (QuantSeq 3' mRNA-Seq FWD, Lexogen). The library was then amplified with 3' PCR primers containing sample indices and the Illumina clustering guides. Indexed libraries were pooled and sequenced on a NextSeq500 (Illumina). Five to ten million single-end 75bp reads were generated as an output. Adaptor trimming was performed, and reads were aligned to the mm10 reference genome using HISAT2.[91] Aligned reads were quantified using HTSeq.[92] Counts were normalized and unwanted variance was removed using RUV-III in R.[93] Differential expression analysis was performed using edgeR.[94] Volcano plots were produced with ggplot2.[95] Heatmaps were generated with z-scores following standardization of log2 normalized counts using the Comple Heatmap library in R.[96]

ScRNA-seq of FACS sorted T cells

AT3-OVA mammary fat pad tumors were harvested from three tumor bearing mice, 2 weeks post BC tumor inoculation (Figure 2). Cells were stained with anti-CD45 APC-CY7 (clone 140; Biolegend) and fixable yellow viability dye. All live, $CD45^+$ TILs were sorted using the BD Fushion 5 sorter. Samples were counted and pooled by treatment group and ~10,000 viable cells were used for further processing. Cell hashing was performed on individual samples using oligo-tagged antibodies (TotalSeq-C0301 anti-mouse Hashtag 1 [barcode sequence: ACCCACCAGTAAGAC], C0302 anti-mouse Hashtag 2 [GGTCGAGAGCATTCA], C0304 anti-mouse Hashtag 4 [AAAGCATTCTTCACG]; Biolegend), according to the manufacturer's instructions. Hashed cells were pooled and processed with the Chromium Controller microfluidic device (10X Genomics), using the Chromium Next GEM Single Cell 5' Kit v2 and Chromium Single Cell Mouse TCR Amplification kit. Pooled libraries were sequenced on a NextSeq (Illumina) targeting 50,000 reads per cell. Sequencing data was demultiplexed, mapped to the murine reference genome/transcriptome (Ensembl release 93 GRCm38) and gene counts were quantified per cell using the Cell Ranger pipeline (version 3.1.0). Multiplet droplets were removed using HTODemux,[97] and genes expressed in <10 cells were filtered out. The filtered UMI count matrix was normalized by sctransform.[98] $CD8^+$ T cells were selected based on high expression of *CD3D*, *CD3E*, *CD3G*, *CD8A* and *CD8B1*. After filtering a total of 1548 single cells remained in the analysis. In order to obtain biologically meaningful clusters, the FindNeighbors function was applied with the *k.para* parameter set at 30, and the FindClusters function was applied with *resolution* of 0.6. Additionally, we calculated a $CD69^+CD103^-$ AUCell signature score[99] for each cell using the raw UMI counts of the 46 genes significantly upregulated in $CD69^+CD103$- cells, and a $CD69^+CD103^+$ AUCell signature score using the raw UMI counts of the 41 genes significantly upregulated in $CD69^+CD103^+$ cells. The upregulated and downregulated signatures were derived from differential expression markers between $CD69^+CD103^-$ and $CD69^+CD103^+$ sub-populations from RNA-seq, which is shown in Figure 1M. The genes used to calculate the signature scores are given in Table S1. A Wilcoxon rank sum test was used to compare the signature score and log normalized expression between $CD8^+TOX^{high}$ cells and $CD8^+ITGAE^+$ cells. The single cell TCR sequences were annotated using the Cell Ranger vdj pipeline (version 3.1.0). The Jaccard index was determined by the number of CDR3 amino acid sequences in each $CD8^+$ T subpopulation. Each individual mouse was analyzed initially which determined that the clonotype overlap between the *Itgae* and *Tox* clusters was not significantly influenced by mouse variability and hence the data was pooled for presentation.

Gene set enrichment analysis

Gene expression datasets in Figures 1 and 2, pertaining to core T_{RM} and exhaustion $CD8^+$ T cell gene signatures were curated from the literature. A unique "$CD8^+$ T_{RM} gene signature" derived from scRNA-seq of tumor infiltrating lymphocytes in human early-stage TNBC tumors (GEO: GSE110686) was derived from Savas et al.[13] A "murine infection residency signature" representing a core T_{RM} transcriptional signature derived from healthy skin, gut, and liver of mice following resolution of viral infection (GEO: GSE70813) was derived from Mackay et al.[44] A murine "Core $CD8^+$ T cell exhaustion (T_{EX}) gene signature" originating from bulk RNA-seq on $CD8^+$ T cells flow sorted from mice with chronic lymphocytic choriomeningitis virus (LCMV) infection (GEO: GSE84820) was derived from Man et al.[61] Progenitor exhausted and terminally exhausted $CD8^+$ T cell signatures derived $CD8^+Slamf6^+Tim\text{-}3^-$ and $CD8^+Slamf6^-Tim\text{-}3^+$ T cells respectively, which underwent bulk RNA-seq after isolation from the spleens of mice subjected to chronic LCMV infection (GEO: GSE123235) was derived from Miller et al.[62] A refined T_{RM} signature was derived based on murine infection models and a $CD8^+$ T cell exhaustion signature from melanoma TIL dataset (GEO: GSE72056) from Jaiswal et al,[64] was utilized in Figure 5. Gene sets from the published gene signature are filtered by FDR < 1% when published as differential expression results. For Figure 5, Human gene homologs were mapped to the mouse genes using the Mouse Genome Informatics Database[100] where required (human gene list in Table S5). These gene sets were used to interrogate the transcriptome of murine BC $CD69^+CD103^-$ and $CD69^+CD103^+$ $CD8^+$ T_{RM}-like cells. GSEA analysis for multiple contrasts was performed using the fgsea library in R.[101] P values were adjusted for multiple hypothesis testing where appropriate. For single contrasts, gene set testing was performed using the 'fry' function and corresponding plots were made using the 'barcode' function from limma.[81] Here the x axis values are the standardized logFC values/rank from the gene in the set subject to testing and the y axis shows the enrichment score.

Survival cohort analyses

In Figure 5, we generated a gene signature that could be applied to human tumor gene expression data, differentially expressed genes between $CD44^{hi}CD8^+CD69^+CD103^-$ and $CD44^{hi}CD8^+CD69^+$ $CD103^+$ T_{RM}-like cells from tumor-free mammary fat pad after dual-ICB therapy at day 40 post TNBC inoculation were used. Following the method from our previous work,[13] we used the differentially expressed genes upregulated in $CD69^+CD103^+$ compared to $CD69^+CD103^-$ D40 $CD8^+$ T cell samples (false discovery rate

(FDR) <1% and log2 fold change >1) to derive a D40 CD8$^+$ T_{RM} signature (Table S5). Human gene homologs were mapped to the mouse genes as described earlier. Tumor biopsies and profiles are generated from the diagnostic-treatment sample. All trial details, patient demographics and clinical data have been previously described in the referenced clinical publications. The prognostic associations of the D40 T_{RM}-like signature were determined in TNBC cases from the METABRIC dataset.[65] The normalized gene expression data and survival data for METABRIC were accessed using CBioPortal[82] and analyzed in R. TNBC samples were classified by the PAM50 molecular subtype classifier. Kaplan–Meier survival curves were generated by partitioning cases in a 50:50 split based on ranked signature expression, which was determined using the 'sig.score' function in the R package genefu (version 2.28.0).[83] Hazard ratios were derived using Cox proportional hazards survival models with endpoints of overall survival and distant-disease-free survival. We then accessed the I-SPY2-990 Dataset (GSE194040) and assessed the performance of the D40 CD8$^+$ T_{RM} signature to predict pathological complete response (pCR) in pembrolizumab ICB treated patients using Area Under the Curve (AUC) Receiver Operating Characteristics curve (ROC) over basal samples. AUC ROC analyses were produced using the library pROC in R[84] and p values calculated with the library verification.[102] All analyses were produced in R version 4.2.1.

The GeparNuevo (NCT02685059) trial was a randomized phase II trial in early stage triple negative breast cancer.[68] Patients were randomized to the anti-PD-L1 agent durvalumab or placebo in addition to nab-paclitaxel followed by epirubicin and cyclophosphamide. The primary endpoint was the pathological complete response rate at surgery following neoadjuvant treatment. Secondary endpoints included distant disease-free survival and overall survival. Survival data at the time of analysis had a median follow up of 43.7 months. RNA-seq of baseline tumor samples was performed with the HTG EdgeSeq Oncology Biomarker panel covering 2549 genes as previously described.[103] RNA-seq data was available for 162 patients out of a total of 174 enrolled in the trial. Of the full D40 T_{RM} signature, 20 genes were available on the biomarker panel (*FOXP3, GZMA, LPL, SLC11A1, CMKLR1, CCL23, CCL15, DAB2, GZMB, CSF1R, ITGAM, STAB1, TGFB1, FES, C3AR1, CD74, SYK, APOL3, SRC, ITGB7).* Due to this reduced gene set, gene signature scores were calculated as a weighted mean with the log2 fold change as the weighting factor. ROC curves were computed for signature scores as predictors of pCR and evaluated by the AUC metric. P values were calculated with a one-sided Wald test setting AUC = 0.5 as the null hypothesis. Survival endpoints were compared between treatment groups using the log rank test and the analyses were performed by the German Breast Cancer Group.

The T_{RM} signature was also applied to two cohorts of patients with advanced melanoma that were treated with immune checkpoint blockade where gene expression data were available. The Liu et al[69] study was chosen as the largest published cohort where patients had anti-PD-1 therapy after prior anti-CTLA-4 (n = 47 with complete clinical and gene expression data). Anti-CTLA-4 naive patients were not included in our analysis. The Gide et al cohort was chosen as the largest published cohort where patients received combination anti-CTLA-4 and anti-PD-1 therapy[34] (n = 31 with complete clinical and gene expression data). Patients who received anti-PD-1 monotherapy were not included in our analysis. Gene expression data at baseline was used in both studies. Clinical and gene expression data for Liu et al[69] (Accession number: phs000452.v3.p1) are available in the publication. Expression data is provided as transcripts per million and was used unmodified. Clinical data for Gide et al are available with the publication, and baseline RNA-seq data was analyzed as follows in brief. Raw sequencing data for baseline samples in this study were downloaded from the Sequencing Read Archive (Bio Project accession: PRJEB23709). Adapters were trimmed with Skewer[104] and gene expression quantified with kallisto[85] (version 0.46.0) using the GRCh38 Ensembl transcriptome reference (release 99). Tximport[86] and limma[81] were used to process and normalize data. limma voom[87] transformed gene counts were z-scored prior to further analysis.

For both datasets in Figure 5, signature scores were calculated for each tumor as the arithmetic mean of the normalized expression of signature genes. ROC analyses were generated with the radiological response of the patient (partial/complete response versus stable/progressive disease) as the 'response' and the signature score as the 'predictor', using the pROC package[84] and p values calculated with the verification library.[102] Curves were plotted with ggplot2.[95] For survival analyses, each study cohort was split by the median signature score into high/low expression groups for comparison. Survival curves were produced with the Kaplan-Meier estimator and compared with the logrank test using the survminer package.[105]

QUANTIFICATION AND STATISTICAL ANALYSIS

Statistical methods were chosen appropriately as per the experimental setup, p values, sample size estimate, standard error and data distribution were indicated in corresponding figure legends. Data was analyzed using GraphPad Prism, version 8 (GraphPad Software Inc., USA) unpaired Student's t test or one-way ANOVA methods were used for *in vitro* experiments shown in Figure 3 and two-tailed Mann-Whitney test, two-way ANOVA with Tukey's multiple comparison test and with significant difference testing for *in vivo* studies are indicated in respective figure legends including p values. For *in vivo* tumor efficacy experiments in Figures 3 and 4, Log ranked (Mantel–Cox) tests were performed to identify survival differences in mice amongst indicated treatment groups.